Partially overlapping guidance pathways focus the activity of UNC-40/DCC along the anteroposterior axis of polarizing neuroblasts

Annabel Ebbing[*], Teije C. Middelkoop[*,1], Marco Betist, Eduard Bodewes and Hendrik C. Korswagen

Hubrecht Institute, Royal Netherlands Academy of Arts and Sciences and University Medical Center Utrecht, Uppsalalaan 8, 3584 CT, Utrecht, The Netherlands. [1]Present address: Biotechnology Center, Technical University Dresden, Tatzberg 47-49, 01307, Dresden, Germany.

*These authors contributed equally.
Corresponding author: r.korswagen@hubrecht.eu

Key words: polarization, Q neuroblast, netrin, UNC-40/DCC, Fat-like cadherin, DPY-19, MIG-21, Caenorhabditis elegans

Summary statement:
The left-right asymmetric polarization of the *C. elegans* Q neuroblasts is mediated through a ligand-independent mechanism that localizes the netrin receptor UNC-40/DCC at the anterior or posterior side of the cell.

Abstract

Directional migration of neurons and neuronal precursor cells is a central process in nervous system development. In the nematode *C. elegans*, the two Q neuroblasts polarize and migrate in opposite directions along the anteroposterior body axis. Several key regulators of Q cell polarization have been identified, including MIG-21, DPY-19/DPY19L1, the netrin receptor UNC-40/DCC, the Fat-like cadherin CDH-4, and CDH-3/Fat, which we describe in this study. How these different transmembrane proteins act together to direct Q neuroblast polarization and migration is still largely unknown. Here, we demonstrate that MIG-21 and DPY-19, CDH-3 and CDH-4, and UNC-40 define three distinct pathways that have partially redundant roles in protrusion formation, but also separate functions in regulating protrusion direction. Moreover, we show that the MIG-21 - DPY-19 and Fat-like cadherin pathways control the localization and clustering of UNC-40 at the leading edge of the polarizing Q neuroblast, and that this is independent of the UNC-40 ligands UNC-6/netrin and MADD-4. Our results provide insight into a novel mechanism for ligand-independent localization of UNC-40 that directs the activity of UNC-40 along the anteroposterior axis.

Introduction

Cell migration plays a central role in the development of the nervous system. For example, migration of neurons and neuronal precursors is required to form the different cortical layers of the vertebrate brain, and neural crests cells migrate throughout the embryo to generate the peripheral nervous system. The Q neuroblasts of the nematode *Caenorhabditis elegans* provide a powerful model system to study neuronal cell migration at single cell resolution in vivo (Middelkoop and Korswagen, 2014). The two Q neuroblasts are generated at the end of embryogenesis as sister cells of the hypodermal seam cell V5 (Sulston and Horvitz, 1977). They are initially located at similar positions (between seam cells V4 and V5) on the left (QL) and right (QR) lateral sides of the animal, but during the first hours of larval development, the two neuroblasts polarize and migrate in opposite directions along the anteroposterior body axis (Fig. S1A). QL extends a protrusion towards the posterior and migrates to a position dorsal to seam cell V5, whereas QR polarizes in the opposite direction and migrates over seam cell V4. Interestingly, this asymmetric polarization and migration is linked to the subsequent response of the Q neuroblast to Wnt ligands (Honigberg and Kenyon, 2000; Middelkoop et al., 2012; Whangbo and Kenyon, 1999). Thus, the polarization and migration of QL towards the posterior initiates canonical, β-catenin dependent Wnt signaling and expression of the target gene *mab-5*. Expression of this Hox gene in turn induces the QL descendants to either arrest their migration (QL.p) or to continue towards a position in the tail (QL.a) (Salser and Kenyon, 1992) (Fig. S1B). The anterior polarization and migration of QR, on the other hand, leads to a non-canonical Wnt signaling response that mediates the long-range migration of the QR descendants to positions in the anterior body region (Mentink et al., 2014; Zinovyeva et al., 2008).

Several genes have been identified that disrupt the asymmetric polarization and migration of the Q neuroblasts. Among these are five genes - *mig-21*, *dpy-19*, *ptp-3*, *cdh-4,* and *unc-40* - that encode transmembrane proteins (Honigberg and Kenyon, 2000; Middelkoop et al., 2012; Schmitz et al., 2008; Sundararajan and Lundquist, 2012; Sundararajan et al., 2014). MIG-21 has no close orthologs in other species, but shares similarity with the netrin co-receptor UNC-5 and semaphorin 5A through its two extracellular thrombospondin repeats. DPY-19 is an evolutionarily conserved multi-pass transmembrane protein, and one of its mammalian orthologs, DPY19L1, is required for the radial migration of glutaminergic neurons in the developing cerebral cortex (Watanabe et al., 2011). Interestingly, it was shown that DPY-19 functions as a c-mannosyltransferase that glycosylates the thrombospondin repeats of UNC-5 and MIG-21 (Buettner et al., 2013). *ptp-3* encodes a LAR-type receptor protein tyrosine phosphatase (RPTP) (Ackley et al., 2005; Harrington et al., 2002). LAR-RPTPs contain extracellular fibronectin type III repeats and immunoglobulin domains, and two

intracellular phosphatase domains. They interact with components of the extracellular matrix and play an important role in axon guidance, synapse development and cell migration (Ackley et al., 2005; Harrington et al., 2002; Um and Ko, 2013). *cdh-4* encodes one of the two Fat-like cadherin orthologs of *C. elegans* (Pettitt, 2005). Fat-like cadherins function in the planar polarization of epithelial tissues (Matis and Axelrod, 2013), in tissue size regulation (Yin and Pan, 2007) and in cell migration (Horne-Badovinac, 2017; Schmitz et al., 2008; Sundararajan et al., 2014). In mammalian cells, Fat1 localizes at the leading edge of migrating cells and is required for directional polarization and protrusive activity at the lamellipodium (Moeller et al., 2004; Tanoue and Takeichi, 2004). *unc-40* encodes an ortholog of the netrin receptor DCC (Chan et al., 1996). UNC-40 and its ligand UNC-6/netrin control the migration of axonal growth cones along the dorsoventral body axis (Wadsworth, 2002). Moreover, UNC-40 is required for the ventral polarization and invasion of the anchor cell during vulva development (Hagedorn et al., 2013; Wang et al., 2014). In addition to netrin-dependent signaling, also ligand-independent functions of UNC-40 have been described. Thus, UNC-40 can interact with the Robo ortholog SAX-3 to potentiate the response of axonal growth cones to the SLT-1/Slt guidance cue (Yu et al., 2002), and signaling of the Wnt ligand EGL-20 through the Frizzled MIG-1 and the Van Gogh ortholog VANG-1 has been shown to influence the localization of UNC-40 in the developing HSN neuron (Tang and Wadsworth, 2014). Interestingly, UNC-40 may also function independently of netrin in the Q neuroblast lineage, as polarization and migration are not affected in *unc-6*/netrin mutants (Honigberg and Kenyon, 2000).

Genetic epistasis experiments have shown that *mig-21*, *dpy-19*, *ptp-3*/Lar and *cdh-4*/Fat have overlapping functions in the polarization and migration of the Q neuroblasts, while *unc-40*/DCC functions in a separate pathway (Middelkoop et al., 2012; Sundararajan and Lundquist, 2012; Sundararajan et al., 2014). Moreover, it was found that there are distinct left-right asymmetric differences in the functional interactions between these regulators. Thus, *unc-40* was shown to act in parallel to *mig-21* and *ptp-3* to mediate posterior migration of QL, while these two pathways may mutually inhibit each other to direct the protrusion of QR towards the anterior (Sundararajan and Lundquist, 2012). Furthermore, *cdh-4* was found to function together with *mig-21* and *ptp-3* in QL, but in both the *unc-40* and *mig-21* - *ptp-3* pathways in QR (Sundararajan et al., 2014). Apart from these genetic interactions, the underlying mechanism that mediates the robust left-right asymmetric polarization of the Q neuroblasts is still largely unknown.

Here, we show that a second Fat-like cadherin, CDH-3, is also required for the correct polarization of the Q neuroblasts. To further define the functional interaction between *cdh-3*, *cdh-4*, *mig-21*, *dpy-19* and *unc-40*, we performed a detailed quantitative analysis of protrusion formation and directional outgrowth in null or strong loss of function mutants. Our results show that *mig-21* - *dpy-19*, *cdh-3* - *cdh-4*, and *unc-40* define three distinct pathways. We found that

the *unc-40* pathway plays a prominent role in the formation of a major, lamellipodium-like protrusion, while the *mig-21* - *dpy-19* pathway and the Fat-like cadherins have additional functions in specifying the direction of the growing protrusion. Moreover, we show that *cdh-4* has cell autonomous as well as non-autonomous functions in protrusion formation and directional outgrowth. Mechanistically, we show that the *mig-21* - *dpy-19* and *cdh-3* - *cdh-4* pathways are required for the ligand-independent localization of UNC-40/DCC at the leading edge of the Q neuroblast protrusion. We conclude that a complex interplay between the three pathways, which acts in part through the localization of UNC-40 at the protrusive front, mediates the left-right asymmetric polarization of the Q neuroblasts.

Results

Quantitative analysis of Q neuroblast polarization and migration reveals distinct functions of UNC-40/DCC, Fat-like cadherins and the transmembrane proteins MIG-21 and DPY-19 in protrusion formation and direction

The Netrin receptor UNC-40/DCC, the transmembrane proteins MIG-21 and DPY-19, and the Fat-like cadherin CDH-4 are required for the left-right asymmetric polarization and migration of the QL and QR neuroblasts (Middelkoop et al., 2012; Schmitz et al., 2008; Sundararajan and Lundquist, 2012; Sundararajan et al., 2014). In addition, we found that a second Fat-like cadherin, CDH-3, is involved in this process, as demonstrated by the effect of *cdh-3* mutation on Q neuroblast polarization and the subsequent migration of the Q cell descendants (Fig. 1B, S1F).

To further examine the function of these transmembrane proteins in polarization and migration, we quantified the effects of strong loss of function or null mutations. The first step in Q neuroblast migration is the formation of a single, lamellipodium-like protrusion that extends towards the anterior in QR and the posterior in QL. To visualize the Q neuroblasts, we used a transgenic marker that labels the plasma-membrane (GFP-PH) and the nucleus (H2B-GFP) of the Q neuroblasts and the lateral hypodermal seam cells (Wildwater et al., 2011) (Fig. 1A, S1C). We measured the ability of the Q cells to form a major lamellipodium-like protrusion, and the direction of this protrusion with respect to the anteroposterior body axis (as defined by a line between the centers of the nuclei of the Q neuroblast and the seam cell V5) (Fig. 1A) (Middelkoop et al., 2012). In wild type animals, QL extends a protrusion towards the dorsal side of V5 (with a predominant angle of 20 - 40^{o}), while QR sends a protrusion over V4 (with an angle between 140 - 160^{o}) (Fig. 1B). During this phase, filopodia-like membrane extensions are formed at the leading edge of the protrusion (Movie 1, 2). In *mig-21(u787)* and *dpy-19(e1314)* mutants, the direction of the QL and QR protrusions was altered. In agreement with previous studies (Middelkoop et al., 2012), we found that 40 - 50% of QL and QR cells

formed a short, broadly shaped protrusion towards the dorsal side (60 - 120º) (Fig. 1B, S1C, D, see Table S1 for statistical analysis), as well as smaller spike-like filopodia in other directions. In 11 - 16% of animals, the QL and QR neuroblasts failed to form a major protrusion. As discussed below, this phenotype was enhanced in the double mutant, indicating that *mig-21* and *dpy-19* have an additional, partially redundant role in protrusion formation. Loss of *cdh-4* also affected protrusion formation (20 - 23% of QL and QR neuroblasts did not form a lamellipodium-like protrusion in *cdh-4(hd40)* mutants) (Fig. 1B, S1C). The effect on protrusion direction was however different from *mig-21* and *dpy-19*. While there was a relatively modest effect on protrusion direction in QL, there was a striking reversal of direction in QR, with 36% of the cells polarizing towards the posterior instead of the anterior. Time-lapse imaging showed increased formation of small ectopic protrusions (Movie 3), and we observed that the major protrusion can collapse and reform in a different direction (Movie 4). In *cdh-3(pk87)* mutants, there was a mild defect in polarization and protrusion direction, but not the reversal in QR polarity that we observed in the *cdh-4* mutant (Fig. 1B, S1C). However, *cdh-3* mutants did show ectopic protrusive activity and instability of the major protrusion (Movie 5). *unc-40(e271)* mutants showed the highest percentage (35 - 37%) of unpolarized cells (Fig. 1B). We found that these unpolarized cells do show protrusive activity, but that these protrusions are unstable and unable to grow into a lamellipodium-like protrusion (Movie 6). In cells that did form a major protrusion, the average length of the protrusion was reduced (Fig. S2B), while the direction of the protrusion was mostly correct (Fig. 1B, S1C, D).

Once the protrusion has fully extended, the cell body follows and QL divides at a position dorsal to V5, and QR at a position dorsal to V4 (Fig. 2A). In agreement with previous studies (Middelkoop et al., 2012; Sundararajan and Lundquist, 2012; Sundararajan et al., 2014), we found that all the mutants showed defects in the migration of the QL and QR cell bodies (Fig. 2B, C). However, the reduction in migration distance was more severe in *mig-21*, *dpy-19* and *cdh-4* mutants than in the *unc-40* and *cdh-3* mutants, which is consistent with the effect of these mutations on protrusions formation and directional outgrowth. Finally, we examined the position of the Q.p descendants (Q.paa and Q.pap, abbreviated as Q.pax) (Fig. S1B), which is linked to initial polarization and migration through the activation of the Wnt dependent anterior or posterior migration pathways (Honigberg and Kenyon, 2000; Middelkoop et al., 2012). Again, there was a strong correlation between the severity of defects in initial polarization and the subsequent left-right asymmetric migration of the Q.pax (Fig. S1F).

Based on these results, we conclude that *unc-40* is predominantly required for the formation of a major lamellipodium-like protrusion, while *mig-21*, *dpy-19* and the Fat-like cadherin *cdh-4* - and to a lesser extent *cdh-3* - have additional functions in controlling the directional outgrowth of the protrusion. As part of this guidance mechanism, *mig-21* and *dpy-*

19 are required for the asymmetric polarization of QL and QR along the anteroposterior body axis, while *cdh-4* is particularly important for the anterior polarization of QR. Finally, as all four mutants showed ectopic protrusive activity, the coordinated function of these different transmembrane proteins is required for the formation of a single major protrusion.

UNC-40/DCC, MIG-21, DPY-19 and CDH-3 act cell-autonomously, while the Fat-like cadherin CDH-4 has both cell-autonomous and non-autonomous roles in Q neuroblast polarization

We and others have previously shown that *mig-21* is expressed in the Q neuroblasts and that it functions cell-autonomously in Q cell polarization and migration (Middelkoop et al., 2012; Sundararajan and Lundquist, 2012). To examine the expression of *dpy-19*, we used CRISPR/Cas9 mediated genome editing to endogenously tag the *dpy-19* gene with *gfp* (Dickinson et al., 2013). We found that the resulting DPY-19::GFP fusion protein is functional (data not shown) and that it is expressed in the QL and QR neuroblasts, the seam cells and the hypodermal syncytium hyp7 (Fig. 3A). The endogenous DPY-19 protein localizes to the nuclear periphery, which is in agreement with earlier studies using DPY-19 overexpression (Honigberg and Kenyon, 2000). To investigate whether DPY-19 is required in the Q cells or the surrounding hypodermal cells, we used the promotor of *egl-17* (Branda and Stern, 2000; Middelkoop et al., 2012) to specifically express *dpy-19* in the Q cell lineage of *dpy-19(e1314)* mutants. Using the final position of the Q.pax cells as a proxy, we found that Q cell specific expression of DPY-19 was sufficient for correct Q neuroblast polarization and migration (Fig. S2D), which was further confirmed using transgenic mosaics (Table S2). We conclude that MIG-21 and DPY-19 both function cell autonomously in the Q neuroblasts, which is consistent with the shared molecular function of the two proteins (Buettner et al., 2013).

Studies with transgenic reporters have shown that *unc-40* is expressed in the Q neuroblast lineage (Honigberg and Kenyon, 2000). To examine the endogenous expression of *unc-40* during Q cell polarization and migration, we used single molecule mRNA fluorescent in situ hybridization (smFISH) (Raj et al., 2008) to quantitatively measure *unc-40* mRNA abundance. At the early L1 larval stage, *unc-40* expression was detected in the nerve ring and the Q neuroblasts (Fig. 3B, S2A). We found that the number of *unc-40* mRNA spots was similar in QL and QR, with a positive correlation between spot abundance and migration distance (QL, $r = 0.4081$, $p < 0.0022$, QR, $r = -0.2838$, $p < 0.0324$) (Fig. 3E), indicating that *unc-40* is symmetrically expressed in the two lineages, and that expression increases during the polarization and migration process. Earlier studies using Q cell specific rescue and tissue-specific RNAi mediated knock-down have shown that *unc-40* functions cell autonomously in the Q cell lineage (Sundararajan and Lundquist, 2012). To corroborate these finding and to generate a tool for robust Q cell specific depletion of UNC-40, we used CRISPR/Cas9

mediated genome editing to insert a ZF1 tag at the carboxy-terminus of UNC-40. This sequence is recognized by ZIF-1, the substrate-binding subunit of a ubiquitin-ligase complex, which targets the tagged protein for proteasomal degradation (Armenti et al., 2014). We found that ubiquitous expression of ZIF-1 induced an uncoordinated phenotype that was similar as observed in the *unc-40* null mutant (data not shown), indicating that the tagged UNC-40 protein is efficiently degraded. Next, we used the *egl-17* promotor to specifically express ZIF-1 in the Q neuroblast lineage. We found that the effect of UNC-40 depletion on protrusion formation, polarization, and the migration of the Q cell and its descendants was similar to the *unc-40* null mutant (Fig. 3H, S3A, B, C), confirming the cell autonomous function of UNC-40 in this process.

We also used smFISH to examine the expression of *cdh-4* and *cdh-3*. Consistent with transgenic reporter studies (Sundararajan et al., 2014), we observed *cdh-4* mRNA spots in the Q neuroblasts, as well as a wide range of other cells, including the neighboring seam and P cells, ventral nerve cord neurons and cells in the head region (Fig. 3C, S2C). In contrast, we found that during the initial polarization and migration phase, *cdh-3* was specifically expressed in the Q neuroblasts, with additional expression only in a few unidentified cells in the head (Fig. 3D, S2B). Similar to *unc-40*, there was no significant difference in expression between QL and QR. Moreover, for both *cdh-3* and *cdh-4*, the expression level correlated with migration distance (*cdh-3* QL, Spearman $r = 0.5765$, $p < 0.0001$, QR, Spearman $r = -0.4838$, $p < 0.0004$; *cdh-4* QL, Spearman $r = 0.3176$, $p < 0.03$, QR, Spearman $r = -0.5070$, $p < 0.0004$), indicating that expression increases during polarization and migration (Fig. 3F, G). To examine the site of action of *cdh-3* and *cdh-4*, we used CRISPR/Cas9 mediated genome editing to insert a ZF1 tag at the carboxy-terminus and depleted the endogenously tagged proteins using Q lineage specific expression of ZIF-1. Depletion of CDH-3 closely phenocopied the mutant phenotype (Fig. 3H, S3A, B, C). A similar effect on protrusion formation was also observed when CDH-4 was depleted from the Q neuroblast lineage (an average of 22 versus 24% of unpolarized cells in *cdh-4(hd40)* and CDH-4 depletion, respectively), but the reversal of QR polarity observed in the *cdh-4* null mutant was strikingly absent (Fig. 3H).

We conclude that MIG-21, DPY-19, UNC-40/DCC and the Fat-like cadherin CDH-3 function cell autonomously in protrusion formation and guidance. CDH-4/Fat, on the other hand, has a dual role, with a cell autonomous function in protrusion formation and a cell non-autonomous function in directing the protrusion of QR towards the anterior.

MIG-21, DPY-19 and the Fat-like cadherins function in parallel to UNC-40/DCC

To examine genetic interactions between the different polarity regulators, we generated compound mutants. For *mig-21* and *dpy-19*, we found that the phenotype of the double mutant was similar to that of the single mutants (Fig. 1C), with a clear dorsal bias in protrusion

direction. The percentage of unpolarized cells was however increased in the double mutant. These results indicate that *mig-21* and *dpy-19* function together in regulating protrusion direction, which is in agreement with previous genetic studies (Middelkoop et al., 2012) and the observation that MIG-21 is a substrate of DPY-19 c-mannosyltransferase activity (Buettner et al., 2013). However, our results suggest that there is also a minor parallel activity in protrusion formation.

Double mutants between *cdh-3* and *cdh-4* were not viable (data not shown), but we found that homozygous offspring of *cdh-4(hd40) cdh-3(pk87)* heterozygotes develop to the L1 stage. Using the final position of the Q.pax as a proxy for Q polarization and migration, we found that the phenotype of the maternally rescued double mutant was indistinguishable from the *cdh-4* single mutant (Fig. S4C). These results indicate that *cdh-3* and *cdh-4* function in a common pathway, in which *cdh-4* has a predominant role.

Next, we combined mutations in the *cdh-3* - *cdh-4*/Fat and *mig-21* - *dpy-19* pathways with *unc-40*/DCC. Since double mutants between *cdh-4* and *unc-40* are not viable (Sundararajan et al., 2014), we used Q lineage specific expression of ZIF-1 to deplete endogenously tagged UNC-40::ZF1 in a *cdh-4(hd40)* mutant background (Fig. 1C). In agreement with a previous study using tissue-specific RNAi (Sundararajan et al., 2014), the combined loss of *cdh-4* and UNC-40 resulted in a strongly enhanced phenotype. Quantification showed that 63% of QL and 71% of QR neuroblasts remained unpolarized. Moreover, the cells that did form a protrusion, no longer showed the posterior bias observed in the *cdh-4* single mutant. Of note, 6% of QL and QR cells polarized at an angle ventral to the anteroposterior body axis, a phenotype that was not observed in the single mutants. As the triple mutant of *mig-21*, *dpy-19* and *unc-40* was also not viable (data not shown), we used a similar approach to deplete UNC-40 from *mig-21(u787) dpy-19(e1314)* double mutants. Again confirming earlier RNAi experiments (Sundararajan and Lundquist, 2012), this resulted in a strongly enhanced phenotype. We found that there is a strong defect in protrusion formation: 79 - 80% of Q cells remained unpolarized (Fig. 1C), leading to a strong reduction in initial migration (Fig. S4A), misorientation of the position Q.a relative to Q.p (Fig. S4D) and almost complete anterior migration of the QR.pax (Fig. S4B). Furthermore, of the approximately 20% of cells that did form a major protrusion, the predominant polarization direction was shifted from dorsal in the *mig-21 dpy-19* double mutant to anterior in the triple mutant (Fig. 1C). Consistent with these static measurements, time-lapse imaging revealed that the Q neuroblasts either show limited protrusive activity (Movie 7), or form a larger protrusion towards the anterior (Movie 8). However, even when a major lamellipodium is formed, we did not observe migration of the cell body.

Taken together, these results show that *mig-21* and *dpy-19*, and the Fat-like cadherins *cdh-3* and *cdh-4* are part of linear genetic pathways that act in parallel to *unc-40*/DCC. Loss of either of these pathways strongly enhances the polarization defect of *unc-40*. However, in Q cells that still form a major protrusion, loss of *cdh-4* and *unc-40* leads to random polarization, while in the absence of *mig-21*, *dpy-19* and *unc-40* the Q cells predominantly polarize towards the anterior.

The asymmetric polarization of QL and QR is independent of centrosome position

The position of the centrosome, and the axis that it forms with the nucleus, is a key polarity determinant in migrating cells (Luxton and Gundersen, 2011). In many migrating cell types, the centrosome is positioned anterior to the nucleus. Here, it forms a microtubule organizing center that mediates polarized vesicular transport to the leading edge and is important for nuclear movement. Using the centrosomal marker CMD-1::GFP (Chai et al., 2012), we have found that in both QL and QR, the centrosome is localized at the anterior side of the nucleus (Fig. 4A, B). A consequence of this symmetric localization is that the centrosome is positioned on the same side as the protrusion in QR, while it is at the opposite side of the nucleus in QL. Measurements of centrosome position - quantified as the angle of the centrosome and the Q cell nucleus with respect to the anteroposterior body axis - revealed that while the centrosome is anterior to the nucleus in both QL and QR, the angle of centrosome position is more variable in QL (Fig. 4C, D, E). We speculate that this variability is related to the posterior polarization of QL, which may induce microtubule pulling forces that influence the position of the centrosome at the opposite side of the nucleus. The average position of the centrosome was not altered in *mig-21*, *dpy-19* or *unc-40* mutants, but variability was increased in QR. Moreover, there was no correlation between centrosome position and protrusion direction in the mutants (Fig. 4F, G). We conclude that the left-right asymmetric polarization of the Q neuroblasts is independent of centrosome position. However, the anterior localization of the centrosome does correlate with the anterior bias in protrusion direction in the absence of the MIG-21 - DPY-19 and UNC-40/DCC pathways, indicating that it may have a function in specifying an anterior ground polarity.

Anterior polarity in the absence of the UNC-40/DCC and MIG-21 - DPY-19 pathways is dependent on CDH-4/Fat

Given the prominent role of CDH-4 in the anterior polarization of QR, we investigated if it is required for the anterior polarization observed in the absence of the MIG-21 - DPY-19 and UNC-40/DCC pathways. Depletion of *mig-21* by RNAi and UNC-40 by ZIF-1 mediated protein depletion in a *cdh-4(hd40)* mutant background resulted in a further increase in the percentage of Q cells that remain unpolarized (Fig. 4H) and failed to migrate (Fig. S4A), as confirmed by

the almost fully penetrant effect on Q.pax migration (Fig. S4B). Importantly, among the 10% of Q cells that did form a protrusion, the anterior bias in polarization direction was lost (Fig. 4H), with cells polarizing in multiple directions, including angles below the anteroposterior body axis. Based on these results, we propose that the cell non-autonomous CDH-4/Fat pathway provides an anteriorly directed ground polarity, which is modified in QL by the MIG-21 - DPY-19 and UNC-40/DCC pathways to mediate posterior polarization.

The MIG-21 - DPY-19 pathway and CDH-4/Fat mediate ligand-independent localization of UNC-40/DCC

UNC-40/DCC is a key driver of actin dependent protrusion formation (Quinn and Wadsworth, 2008). Studies of migrating neuronal growth cones (Kulkarni et al., 2013) and the polarization and invasion of the anchor cell during vulva formation (Wang et al., 2014) have shown that UNC-40 randomly clusters along the plasma membrane through an interlocked positive and negative feedback mechanism. Directional binding of the ligand UNC-6/netrin stabilizes these clusters and thereby induces protrusive activity at the appropriate side of the cell. Our observation that the Q neuroblasts frequently remain unpolarized in *unc-40* mutants demonstrates that UNC-40 is also an important mediator of protrusion formation during Q cell polarization (Fig. 1B). Interestingly, however, it has previously been shown that the ligand UNC-6/netrin is not required (Honigberg and Kenyon, 2000). To corroborate these findings and to investigate the role of the alternative UNC-40 ligand MADD-4 (Chan et al., 1996; Tu et al., 2015), we examined protrusion formation and direction in *unc-6(ev400)* and *madd-4(kr270)* single and double mutants. Loss of *unc-6* and *madd-4* did not significantly affect protrusion formation, direction and migration (Fig. 5A, S5A, B), supporting the notion that UNC-40 functions ligand-independently in Q neuroblast polarization.

To examine the subcellular localization of UNC-40, we endogenously tagged UNC-40 with GFP using CRISPR/Cas9 mediated genome editing. The carboxy-terminal fusion of UNC-40 with GFP was functional (Fig. S6A), and consistent with *unc-40* mRNA expression (Fig. 3A, E), UNC-40::GFP expression increased during Q cell polarization and migration (Fig. S6B). The endogenous UNC-40::GFP protein localized diffusely along the plasma membrane, but also formed prominent punctate clusters at the cell periphery (Fig. 5B). Consistent with the role of UNC-40 in protrusion formation, quantification showed that these UNC-40 clusters predominantly localize at the leading edge of the polarizing Q cell (Fig 5B, E). Of note, we found that these clusters dissolve when the Q neuroblast divides, but reappear at the leading edge of the migrating daughter cells QR.a and QR.p (Fig. S6B).

In the anchor cell, random clustering of UNC-40 in the absence of the UNC-6/netrin ligand leads to the formation of multiple, unstable and randomly directed protrusions (Wang et al., 2014). Since *mig-21*, *dpy-19* and *cdh-4* mutants also display such ectopic spike-like protrusions, we investigated whether these genes are required for the stabilization and polarized localization of UNC-40. We found that in both *mig-21(u787) dpy-19(e1414)* double mutants and *cdh-4(hd40)* single mutants, the specific localization of UNC-40 at the anterior or posterior side of the Q neuroblast was lost (Fig. 5C, D). Quantification showed dispersed localization of UNC-40 clusters along the Q cell membrane, and a clear reduction in the ratio of clusters at the anterior versus posterior side of the cell (Fig. 5E). In addition, we found that membrane localization and clustering of UNC-40 was significantly increased in *mig-21 dpy-19* double mutants, while it was decreased in *cdh-4* mutants (Fig. 5E, F), indicating that the two pathways also have distinct functions in controlling the localization or stability of UNC-40 at the cell membrane.

Taken together, these results support the notion that the MIG-21 - DPY-19 and the CDH-4/Fat pathways are part of a novel ligand-independent mechanism that controls the polarized activity of UNC-40.

The MIG-21 - DPY-19 pathway prevents the Q neuroblasts from responding to an UNC-6/netrin dependent dorsalizing signal

The UNC-40 ligand UNC-6/netrin plays a central role in polarization and migration along the dorsoventral axis (Wadsworth, 2002). Interestingly, we observed a prominent dorsal bias in protrusion direction in the *mig-21 dpy-19* single and double mutants (Fig. 1B, C). Since this dorsal polarization is dependent on UNC-40 (Fig. 1C), we investigated if loss of the MIG-21 - DPY-19 pathway triggers an ectopic response to UNC-6. We generated a *mig-21 dpy-19*; *unc-6(ev400)* triple mutant and found that loss of *unc-6* strongly suppressed dorsal polarization (from 36 - 44% to 16%, $p < 0.01$), with a clear shift towards posterior polarization in QL and anterior polarization in QR (Fig. 5A), an increase in migration distance (Fig. S5A) (with a concomitant increase in Q.a and Q.p mispositioning, Fig. S5C), and a partial rescue of QR.pax migration (Fig. S5B). These results show that the Q neuroblasts can respond to UNC-6, but that this response is normally prevented by the MIG-21 - DPY-19 pathway. This is consistent with a role of the MIG-21 - DPY-19 pathway in localizing UNC-40 at the leading edge, and supports the model that the MIG-21 - DPY-19 and CDH-4/Fat pathways are part of a ligand independent mechanism that redirects the activity of UNC-40 from the dorsoventral to the anteroposterior body axis.

Discussion

The MIG-21 - DPY-19, CDH-3 - CDH-4/Fat and UNC-40/DCC pathways separately control directional outgrowth of the Q neuroblast protrusion

The transmembrane proteins MIG-21, DPY-19, CDH-4/Fat and UNC-40/DCC play a central role in the left-right asymmetric polarization and migration of the Q neuroblasts (Middelkoop et al., 2012; Schmitz et al., 2008; Sundararajan and Lundquist, 2012; Sundararajan et al., 2014). Previous studies have suggested that CDH-4 acts together with MIG-21 and UNC-40 in the anterior polarization of QR, while it functions in parallel to UNC-40 in the posterior polarization of QL (Sundararajan et al., 2014). Our detailed quantitative analysis shows that these interactions are more complex. We found that *unc-40*/DCC, *mig-21* and *dpy-19*, and *cdh-4*/Fat and *cdh-3* - the Fat-like cadherin gene identified in this study - represent three separate genetic pathways that control distinct aspects of the polarization process. Thus, in *unc-40*/DCC mutants, the direction of polarization is more variable than in wild type. In *mig-21* and *dpy-19* single or double mutants, there is a clear dorsal bias in polarization. Finally, in *cdh-4*/Fat mutants, there is an increased variability in polarization direction and a striking reversal in the polarity of QR. This polarity reversal is not observed in *cdh-3* mutants, but double mutant analysis indicates that both Fat-like cadherins are part of the same pathway. Interestingly, we have found that Q lineage specific depletion of CDH-4 did not reproduce the reversal in QR polarity observed in the null mutant, indicating that this is a cell non-autonomous function of CDH-4. This is consistent with previous mosaic rescue experiments (Sundararajan et al., 2014) and is in agreement with the expression of *cdh-4* in neighboring seam cells and juvenile ventral cord neurons. Cadherin family members can form homo- or heterotypic interactions through their extracellular domains (Gooding et al., 2004), and similar interactions between CDH-4, CDH-3 and other cadherin-related proteins such as CDH-1 may underlie the cell non-autonomous function of CDH-4 in QR polarization. Moreover, as has been described for dFat2 in collective cell migration in *Drosophila*, where dFat2 stabilizes Lar at the leading edge of neighboring cells (Barlan et al., 2017), CDH-4 may interact with PTP-3/Lar to promote anterior polarization of the Q neuroblasts.

The parallel function of the three pathways is also demonstrated in mutant combinations. Depletion of UNC-40 in a *mig-21*; *dpy-19* double mutant background resulted in a strong defect in protrusion formation, which is discussed below. Interestingly, in cells that did form a major lamellipodium, the polarization direction was predominantly anterior. This anterior bias is correlated with the position of the centrosome, which is located anterior to the nucleus in both QL and QR. The symmetric localization of the centrosome derives from the division of the hypodermal QLV5L and QRV5R precursor cells that generate the two Q neuroblasts (as anterior daughters that both inherit an anterior centrosome) and their sister

cells, the seam cells V5L and V5R (the posterior daughters with a posterior centrosome, data not shown) (Sulston et al., 1983). In migrating cells, the centrosome is often localized at the front of the nucleus, and it is thought that this contributes to the formation of a polarized microtubule network that transports components of the cell polarity and migration machinery to the leading edge of the cell (Etienne-Manneville, 2013; Luxton and Gundersen, 2011). Although centrosome position did not correlate with protrusion direction in QL and QR, it may contribute to the anterior bias that emerges in the absence of the MIG-21 - DPY-19 and UNC-40 pathways. Such an anterior ground polarity may also be linked to the non-cell autonomous activity of CDH-4. Thus, loss of *cdh-4* predominantly affects the anterior polarization of QR, and the anterior bias observed in the absence of the MIG-21 - DPY-19 and UNC-40 pathways is lost when CDH-4 is depleted. An intriguing possibility is therefore that the CDH-4 pathway links centrosome position with anterior polarization in QR, while this activity is modulated or overruled to allow posterior polarization in QL.

The UNC-40/DCC, CDH-3 - CDH-4/Fat and the MIG-21 - DPY-19 pathways are required for the formation of a major, lamellipodium-like protrusion

We found that UNC-40/DCC has a prominent role in protrusion formation. In *unc-40* mutants, the Q neuroblasts frequently fail to form a major protrusion. This is also observed when UNC-40 is specifically depleted from the Q cell lineage, indicating that UNC-40 acts cell autonomously in this process. UNC-40 is an established regulator of protrusion formation in axonal growth cones and the directional outgrowth of invasive protrusions of the anchor cell during vulva development (Quinn and Wadsworth, 2008; Wang et al., 2014). Consistent with a direct function in protrusion formation, we found that endogenous UNC-40 specifically localizes at the leading edge of the Q cell protrusion. Although the intracellular effectors of UNC-40 vary in different cellular contexts, UNC-40 has been shown to act upstream of various regulators of actin dynamics, including the actin binding protein UNC-115/AbLIM, the Rho family GTPase CED-10/Rac1 and its regulators TIAM-1 and UNC-73/Trio (Demarco et al., 2012; Yu et al., 2002), and UNC-34, an ortholog of the enabled/vasodilator-stimulated phosphoprotein (Ena/VASP), a key mediator of actin filament formation in migrating cells and growth cones (Gitai et al., 2003). Of these, CED-10/Rac1, UNC-73/Trio and UNC-34/Ena are required for Q cell migration (Dyer et al., 2010; Shakir et al., 2006), indicating that UNC-40 may signal through a CED-10/Rac1 and UNC-34/Ena dependent mechanism to form a major protrusion.

The Fat-like cadherins CDH-4, and to a lesser extent CDH-3, are also required for protrusion formation. Depletion of CDH-4 from the Q cell lineage revealed that this function is cell autonomous, demonstrating that - in addition to its cell non-autonomous function in specifying protrusion direction - it is also required in the Q neuroblasts for protrusion formation.

To date, no downstream effectors of CDH-3 and CDH-4 have been identified. Studies in mammalian cells have shown that Fat1 binds Ena/VASP through a proline-rich class I EVH1 domain (Moeller et al., 2004; Tanoue and Takeichi, 2004). Interestingly, a consensus PPxxF class II type EVH1 binding motif is present in the intracellular domain of CDH-4 and this domain is directly adjacent to another proline-rich motif (PVVPPPL) (Schmitz et al., 2008), indicating that CDH-4 may act through an UNC-34/Ena dependent mechanism as well.

mig-21 and *dpy-19* single mutants show only a slight defect in protrusion formation, but this phenotype is enhanced in the double mutant, indicating that the two genes have a partial, non-overlapping function in regulating protrusive activity. Loss of *mig-21* and *dpy-19* also strongly enhances the defect in protrusion formation when UNC-40 is depleted or when depletion of UNC-40 is combined with loss of *cdh-4*. MIG-21 is a thrombospondin repeat containing protein that is modified by the c-mannosyltransferase activity of DPY-19 (Buettner et al., 2013). How MIG-21 and DPY-19 are involved in protrusion formation is not known, but based on genetic epistasis analysis, *mig-21* acts in the same pathway as *ptp-3*/Lar (Sundararajan and Lundquist, 2012). LAR-type RPTPs functionally interact with some of the same actin regulators (such as Trio and ENA/VASP) (Um and Ko, 2013) that act downstream of UNC-40/DCC and possibly CDH-4. Consistent with such potential overlap in downstream effectors, the three pathways act partially redundantly, with strong synergistic interactions when both the MIG-21 - DPY-19 and UNC-40 or CDH-4 and UNC-40 pathways are depleted. We speculate that cross-talk at the level of shared downstream effectors may integrate the activity of the three pathways in protrusion formation and link it to the directional outgrowth mechanisms discussed above.

A ligand-independent function of UNC-40/DCC in Q neuroblast polarization

Previous studies on axon outgrowth and anchor cell polarization have shown that UNC-40 randomly clusters along the plasma membrane through an interlocked positive and negative feedback mechanism (Kulkarni et al., 2013; Wang et al., 2014). These spontaneously formed clusters are sufficient to form small protrusions, but for the formation of a larger, lamellipodium-like protrusion, these clusters need to be stabilized. Such stabilization can be mediated through binding of the ligand UNC-6/netrin, which forms a ventral to dorsal gradient and polarizes protrusive activity along this axis (Wadsworth, 2002). UNC-6 can act in a concentration-dependent manner to promote outgrowth of the protrusion towards (or away from) its source of expression. Recent studies have shown that directionality can also be achieved through a stochastic mechanism in which extracellular cues act in a concentration-independent manner to influence the probability of UNC-40 localization and protrusion formation at a specific side of the cell (Limerick et al., 2018; Wadsworth, 2018). Interestingly, it has previously been shown that UNC-40 acts independently of UNC-6/netrin in Q neuroblast

polarization (Honigberg and Kenyon, 2000). We could confirm these observations, and show that protrusion formation is also unaffected by loss of the alternative UNC-40 ligand MADD-4 or the combined loss of both ligands. Although we cannot rule out the possibility that another, as yet unidentified netrin-like ligand may be involved, these results strongly suggest that UNC-40 functions in a ligand-independent manner.

Endogenous UNC-40 forms distinct punctate clusters at the leading edge of the Q cell protrusion. We found that this highly polarized localization is dependent on the MIG-21 - DPY-19 and CDH-4/Fat pathways. Thus, in *mig-21 dpy-19* double mutants and *cdh-4* single mutants, the UNC-40 clusters are still formed, but their localization is more dispersed along the Q neuroblast membrane. Consistently, we found that the Q neuroblasts form multiple ectopic, filipodia-like protrusions in these mutant backgrounds. Based on these results, we propose that the MIG-21 - DPY-19 and CDH-4/Fat pathways have a dual function in protrusion formation. As discussed above, both pathways can directly promote protrusion formation, explaining why double mutants between these pathways and *unc-40* display an enhanced defect in outgrowth activity. However, our results show that the two pathways also provide a ligand-independent mechanism for localized UNC-40 stabilization. Such a ligand-independent mechanism may be necessary to focus the activity of UNC-40 along the anteroposterior axis, instead of the dorsoventral axis that is specified by the UNC-6/netrin gradient. In support of such a model is our observation that the Q neuroblasts polarize towards the dorsal side in *mig-21 dpy-19* double mutants, and that this dorsal bias is lost in the absence of *unc-6*.

An important question is how the MIG-21 - DPY-19 and CDH-4/Fat pathways control the asymmetric localization of UNC-40, and how this is linked to their own function in polarity establishment. Several mechanisms have been proposed that can localize and polarize the activity of guidance receptors like UNC-40. In canonical chemoattraction a concentration gradient of an extracellular cue results in polarization and activation of its receptor along this gradient (Tessier-Lavigne and Goodman, 1996). Alternatively, receptor activation may be aligned with cell intrinsic polarity axes without the need of direct extracellular guidance cues (Limerick et al., 2018; Wadsworth, 2018). Although we cannot discriminate between these possibilities, our observation that the polarization of the Q neuroblasts is mainly a cell autonomous process - which is modified by extracellular CDH-4/Fat to achieve anterior polarization of QR - may favor the latter possibility. Given the evolutionary conservation of DPY-19, PTP-3/LAR and the Fat-like cadherins, ligand-independent UNC-40/DCC stabilization through these transmembrane proteins may provide a general mechanism for uncoupling UNC-40/DCC signaling from netrin guidance cues.

Materials and Methods

C. elegans strains and culture

Unless noted otherwise, *C. elegans* strains were cultured at 20°C using standard conditions (Lewis and Fleming, 1995). The Bristol N2 strain was used as wild type. The alleles and transgenes used in this study are LGI: *unc-40(e271)* (Brenner, 1974); *unc-40(hu242[unc-40::gfp^flag3x])*, *unc-40(hu226[unc-40::zf1]),* LGII: *muIs32[Pmec-7::gfp; lin-15(+)]* (Ch'ng et al., 2003); *madd-4(kr270)* (Seetharaman et al., 2011), LGIII: *cdh-4(hd40)* (Schmitz et al., 2008), *cdh-4(hu240[cdh-4::zf1])*, *mig-21(u787)* (Du and Chalfie, 2001), *cdh-3(pk87)* (Pettitt et al., 1996), *cdh-3(hu238[cdh-3::zf1])*, *dpy-19(e1314)* (Honigberg and Kenyon, 2000), *dpy-19(hu257[dpy-19::gfp^SEC^flag3x]),* LGIV: *dpy-20(e1362),* LGV: *heIs63[Pwrt-2::gfp-ph; Pwrt-2::h2b::gfp; Plin-48::tomato]* (Wildwater et al., 2011), LGX: *unc-6(ev400), huIs166[Pwrt-2::h2b::mcherry; Pwrt::ph::mcherry; dpy-20(+)]*, and linkage group unknown: *casIs22[Pegl-17::GFP-TEV-S-cmd-1; Pegl-17::myri-mcherry; Pegl-17::mcherry-TEV-S-his-23; rol-6(dn)]* (Chai et al., 2012), *huIs181 [Pegl-17::zif-1-SL2-mcherry; Pmyo-2::mcherry]*. The following extrachromosomal arrays were generated: *huEx439[Pegl-17::dpy-19; Pmyo-2::gfp]*, *huEx440[Pegl-17::dpy-19; Pmyo-2::gfp]*. We used hT2(I:III)[let-? qIs48] to generate a balanced *cdh-4 cdh-3/hT2* strain. As recombination is not fully suppressed in this strain, all animals examined were checked by PCR for presence of the *cdh-4* allele. Strains containing *dpy-19(e1314)* were grown at 15°C, but were shifted to 20°C a day prior to analysis. Synchronized populations of animals were obtained by collecting L1 larvae 0-1 hours after hatching and growing them for 1 hour for protrusion formation and directionality assays, 2 hours for the analysis of centrosome position, 4-6 hours for the position of the first Q neuroblast division, and 12 hours for determining Q.pax position.

Microscopy and fluorescence quantification

For confocal, epifluorescence and DIC microscopy, animals were mounted on 2% agarose pads containing 10 mM sodium azide. Static imaging of Q neuroblast polarization, migration, and the position of the first division were performed on a Zeiss Axioscop with Axiocam camera and images were processed using ImageJ and Adobe Photoshop (Middelkoop et al., 2012). For imaging endogenous DPY-19::GFP, a PerkinElmer Ultraview Vox spinning disk confocal microscope (100x objective, 77.5% 488nm laser power, exposure 800 msec, 9% 561nm laser power, exposure 600 msec) was used. For UNC-40::GFP the settings were 100x objective, 7% 488nm laser power, exposure 800ms, 2% 561nm laser power, exposure 500ms, 0.33 μm z-stack. To quantify membrane associated UNC-40::GFP, line scans (counter clock-wise or clockwise starting from the point of contact with the neighboring anterior or posterior seam cell for QR and QL, respectively) were made using ImageJ. After background subtraction, average

GFP intensity plus 1x standard deviation in wild type was used to define UNC-40::GFP clusters in images of wild type and mutant Q neuroblasts. GFP clusters were divided proportionally to the line scan to determine clusters on the anterior versus the posterior side of the cell. To determine membrane GFP localization, average fluorescence at the membrane was divided by the average fluorescence of a line scan through the cytoplasm.

Time lapse imaging

Samples for live imaging were prepared as previously described (Middelkoop et al., 2012). Animals were imaged using a PerkinElmer Ultraview Vox spinning disk confocal microscope (100x objective, 2-6% 488nm laser power (gradually increasing from 2% to 6% during the course of the experiment), exposure 500 msec, 0.5 μm z-stack). Z-stacks were made every minute, for approximately 300 minutes, using Volocity software. For the *unc-40::zf1, mig-21(u787) dpy-19(e1314), Pegl-17::zif-1* strain, z-stacks were made every 10 minutes. Image sequences were made by selecting z-slices every time point in which the Q neuroblast was in focus. Movies were then processed from image sequences using ImageJ software. To compensate for movement, individual time frames were first aligned with respect to the Q cell nucleus using a normalized cross correlation in a custom-written Matlab script. Subsequently, stacks were further aligned in Fiji by a rigid body transformation using the StackReg plugin (Thevenaz et al., 1998).

Single molecule fluorescence in situ hybridization

smFISH was performed as described (Raj et al., 2008). In short, wild type animals carrying the *heIs63* transgene were synchronized 0-5 hours after hatching and fixed using 4% formaldehyde and 70% ethanol. Hybridization was done for >12 hours at 37°C. *unc-40, cdh-4,* and *cdh-3* oligonucleotide probes were designed using the web-based algorithm at www.singlemoleculefish.com and chemically coupled to Cy5. Z-stacks of 0.5 μm step-size were collected using a Leica DM6000 microscope equipped with a Leica DFC360FX camera, 100x objective and a Y5 filter cube (Cy5). Images were further analyzed and processed with ImageJ software. Quantification was performed as described (Middelkoop et al., 2012), by manually counting mRNA spots in Q neuroblasts, defined by the *heIs63* transgene. Only fluorescent spots visible in at least two neighboring z-slices (0.5 μm step size) were counted.

Quantification of Q neuroblast polarization, migration and centrosome position

Protrusion formation, direction and the position of the first division were quantified as described (Middelkoop et al., 2012). The final position of the Q.pax was determined relative to the seam cells using DIC microscopy (Coudreuse et al., 2006) or by epifluorescence using the *muIs32* (Ch'ng et al., 2003) or *huIs181* transgenes. In some experiments, the final position of the Q descendants AVM (QR.paa) and PVM (QL.paa) were scored relative to the developing vulva in L4 animals using the *muIs32* transgene. The centrosome was visualized using the *casIs22* transgene (Chai et al., 2012). The position of the centrosome was quantified relative to the anteroposterior body axis, and the position of the centrosome with respect to the direction of the protrusive front was determined by measuring the angle of the protrusion with the anteroposterior axis and subtracting the angle made by the centrosome.

Q lineage specific expression of *dpy-19*

The *dpy-19* coding sequence was amplified from cDNA using primers *dpy-19* FW and *dpy-19* RV (Table S3). The PCR product was cloned into pDONR221 using Gateway technology. *Pegl-17::dpy-19::unc-54-3'UTR* was generated by 3-way Gateway cloning of the *eg-17* promotor, *dpy-19* coding sequence and the *unc-54* 3' UTR (Middelkoop et al., 2012) entry clones into the destination vector pCFJ150. The *Pegl-17::dpy-19::unc-54 3' UTR* plasmid was injected at 10 ng/μl together with *Pmyo-2::GFP* (5 ng/μl) and pBluescriptII (135 ng/μl) into *dpy-19(e1314)* mutants. Two independent transgenic lines (*huEx439* and *huEx440*) were isolated and used in this study.

CRISPR/Cas9 mediated genome editing

A zf1 tag was inserted at the carboxy-terminus of *unc-40*, *cdh-4* and *cdh-3* using single stranded oligo DNA (ssODN) repair templates as described (Arribere et al., 2014; Paix et al., 2015). Sequences of the guide RNAs and repair templates are in Table S3. For inserting GFP at the carboxy-terminus of *unc-40* and *dpy-19*, the previously described self-excising cassette (SEC) approach was used (Dickinson et al., 2015). sgRNAs were generated by *in vitro* transcription from PCR fragments containing the T7 promotor and the sgRNA sequence of interest. Primers to generate the PCR fragments for sgRNA synthesis and the homology arms are in Table S3. The homology arms were cloned into the GFP containing vector pDD282 as described (Dickinson et al., 2015). Guide RNAs and repair templates were co-injected with recombinant SpCas9 (D'Astolfo et al., 2015) as described (Arribere et al., 2014; Paix et al., 2015).

Statistical analysis

Protrusion formation and directionality, position of division, and Q.pax localization were compared using Fisher's exact test (Table S1) or Student's t-test as indicated. The correlation between smFISH spot abundance and migration distance was calculated using Spearman's rank correlation coefficient. For centrosome position, Levene's test was performed to address homogeneity of variance. To compare the number of UNC-40::GFP clusters on the anterior versus the posterior side of wild type and mutant Q neuroblasts, Tukey's multiple comparison tests were performed. The membrane UNC-40::GFP localization was compared using the Holm-Sidak's multiple comparisons test.

Acknowledgements

We thank members of the Korswagen group for critically reading the manuscript, the Hubrecht Imaging Center (HIC) for assistance with microscopy and the Utrecht University Gene Editing Facility for recombinant SpCas9 protein. Some strains were provided by the CGC, which is funded by the NIH Office of Research Infrastructure Programs (P40 OD010440). This work was funded by the research program 14NOISE01 of the Foundation for Fundamental Research on Matter (FOM), which is financially supported by the Netherlands Organization for Scientific Research (NWO).

References

Ackley, B.D., Harrington, R.J., Hudson, M.L., Williams, L., Kenyon, C.J., Chisholm, A.D., and Jin, Y. (2005). The two isoforms of the *Caenorhabditis elegans* leukocyte-common antigen related receptor tyrosine phosphatase PTP-3 function independently in axon guidance and synapse formation. J Neurosci **25**, 7517-7528. doi: 10.1523/JNEUROSCI.2010-05.2005

Armenti, S.T., Lohmer, L.L., Sherwood, D.R., and Nance, J. (2014). Repurposing an endogenous degradation system for rapid and targeted depletion of *C. elegans* proteins. Development **141**, 4640-4647. doi: 10.1242/dev.115048

Arribere, J.A., Bell, R.T., Fu, B.X., Artiles, K.L., Hartman, P.S., and Fire, A.Z. (2014). Efficient marker-free recovery of custom genetic modifications with CRISPR/Cas9 in *Caenorhabditis elegans*. Genetics **198**, 837-846. doi: 10.1534/genetics.114.169730

Barlan, K., Cetera, M., and Horne-Badovinac, S. (2017). Fat2 and Lar define a basally localized planar signaling system controlling collective cell migration. Dev Cell **40**, 467-477 e465. doi: 10.1016/j.devcel.2017.02.003

Branda, C.S., and Stern, M.J. (2000). Mechanisms controlling sex myoblast migration in *Caenorhabditis elegans* hermaphrodites. Dev Biol **226**, 137-151. doi: 10.1006/dbio.2000.9853

Brenner, S. (1974). The genetics of *Caenorhabditis elegans*. Genetics **77**, 71-94.

Buettner, F.F., Ashikov, A., Tiemann, B., Lehle, L., and Bakker, H. (2013). *C. elegans* DPY-19 is a C-mannosyltransferase glycosylating thrombospondin repeats. Mol Cell **50**, 295-302. doi: 10.1016/j.molcel.2013.03.003

Ch'ng, Q., Williams, L., Lie, Y.S., Sym, M., Whangbo, J., and Kenyon, C. (2003). Identification of genes that regulate a left-right asymmetric neuronal migration in *Caenorhabditis elegans*. Genetics **164**, 1355-1367.

Chai, Y., Li, W., Feng, G., Yang, Y., Wang, X., and Ou, G. (2012). Live imaging of cellular dynamics during *Caenorhabditis elegans* postembryonic development. Nat Protoc **7**, 2090-2102. doi: 10.1038/nprot.2012.128

Chan, S.S., Zheng, H., Su, M.W., Wilk, R., Killeen, M.T., Hedgecock, E.M., and Culotti, J.G. (1996). UNC-40, a *C. elegans* homolog of DCC (Deleted in Colorectal Cancer), is required in motile cells responding to UNC-6 netrin cues. Cell **87**, 187-195.

Coudreuse, D.Y., Roel, G., Betist, M.C., Destree, O., and Korswagen, H.C. (2006). Wnt gradient formation requires retromer function in Wnt-producing cells. Science **312**, 921-924. doi: 10.1126/science.1124856

D'Astolfo, D.S., Pagliero, R.J., Pras, A., Karthaus, W.R., Clevers, H., Prasad, V., Lebbink, R.J., Rehmann, H., and Geijsen, N. (2015). Efficient intracellular delivery of native proteins. Cell **161**, 674-690. doi: 10.1016/j.cell.2015.03.028

Demarco, R.S., Struckhoff, E.C., and Lundquist, E.A. (2012). The Rac GTP exchange factor TIAM-1 acts with CDC-42 and the guidance receptor UNC-40/DCC in neuronal protrusion and axon guidance. PLoS Genet **8**, e1002665. doi: 10.1371/journal.pgen.1002665

Dickinson, D.J., Pani, A.M., Heppert, J.K., Higgins, C.D., and Goldstein, B. (2015). Streamlined genome engineering with a self-excising drug selection cassette. Genetics **200**, 1035-1049. doi: 10.1534/genetics.115.178335

Dickinson, D.J., Ward, J.D., Reiner, D.J., and Goldstein, B. (2013). Engineering the *Caenorhabditis elegans* genome using Cas9-triggered homologous recombination. Nat Methods **10**, 1028-1034. doi: 10.1038/nmeth.2641

Du, H., and Chalfie, M. (2001). Genes regulating touch cell development in *Caenorhabditis elegans*. Genetics **158**, 197-207.

Dyer, J.O., Demarco, R.S., and Lundquist, E.A. (2010). Distinct roles of Rac GTPases and the UNC-73/Trio and PIX-1 Rac GTP exchange factors in neuroblast protrusion and migration in *C. elegans*. Small GTPases **1**, 44-61. doi: 10.4161/sgtp.1.1.12991

Etienne-Manneville, S. (2013). Microtubules in cell migration. Annu Rev Cell Dev Biol **29**, 471-499. doi: 10.1146/annurev-cellbio-101011-155711

Gitai, Z., Yu, T.W., Lundquist, E.A., Tessier-Lavigne, M., and Bargmann, C.I. (2003). The netrin receptor UNC-40/DCC stimulates axon attraction and outgrowth through enabled and, in parallel, Rac and UNC-115/AbLIM. Neuron **37**, 53-65.

Gooding, J.M., Yap, K.L., and Ikura, M. (2004). The cadherin-catenin complex as a focal point of cell adhesion and signalling: new insights from three-dimensional structures. Bioessays **26**, 497-511. doi: 10.1002/bies.20033

Hagedorn, E.J., Ziel, J.W., Morrissey, M.A., Linden, L.M., Wang, Z., Chi, Q., Johnson, S.A., and Sherwood, D.R. (2013). The netrin receptor DCC focuses invadopodia-driven basement membrane transmigration in vivo. J Cell Biol **201**, 903-913. doi: 10.1083/jcb.201301091

Harrington, R.J., Gutch, M.J., Hengartner, M.O., Tonks, N.K., and Chisholm, A.D. (2002). The *C. elegans* LAR-like receptor tyrosine phosphatase PTP-3 and the VAB-1 Eph receptor tyrosine kinase have partly redundant functions in morphogenesis. Development **129**, 2141-2153.

Honigberg, L., and Kenyon, C. (2000). Establishment of left/right asymmetry in neuroblast migration by UNC-40/DCC, UNC-73/Trio and DPY-19 proteins in *C. elegans*. Development **127**, 4655-4668.

Horne-Badovinac, S. (2017). Fat-like cadherins in cell migration-leading from both the front and the back. Curr Opin Cell Biol **48**, 26-32. doi: 10.1016/j.ceb.2017.04.003

Kulkarni, G., Xu, Z., Mohamed, A.M., Li, H., Tang, X., Limerick, G., and Wadsworth, W.G. (2013). Experimental evidence for UNC-6 (netrin) axon guidance by stochastic fluctuations of intracellular UNC-40 (DCC) outgrowth activity. Biol Open **2**, 1300-1312. doi: 10.1242/bio.20136346

Lewis, J.A., and Fleming, J.T. (1995). Basic culture methods. Methods Cell Biol **48**, 3-29.

Limerick, G., Tang, X., Lee, W.S., Mohamed, A., Al-Aamiri, A., and Wadsworth, W.G. (2018). A statistically-oriented asymmetric localization (SOAL) model for neuronal outgrowth patterning by *Caenorhabditis elegans* UNC-5 (UNC5) and UNC-40 (DCC) netrin receptors. Genetics **208**, 245-272. doi: 10.1534/genetics.117.300460

Luxton, G.W., and Gundersen, G.G. (2011). Orientation and function of the nuclear-centrosomal axis during cell migration. Curr Opin Cell Biol **23**, 579-588. doi: 10.1016/j.ceb.2011.08.001

Matis, M., and Axelrod, J.D. (2013). Regulation of PCP by the Fat signaling pathway. Genes Dev **27**, 2207-2220. doi: 10.1101/gad.228098.113

Mentink, R.A., Middelkoop, T.C., Rella, L., Ji, N., Tang, C.Y., Betist, M.C., van Oudenaarden, A., and Korswagen, H.C. (2014). Cell intrinsic modulation of Wnt signaling controls neuroblast migration in *C. elegans*. Dev Cell **31**, 188-201. doi: 10.1016/j.devcel.2014.08.008

Middelkoop, T.C., and Korswagen, H.C. (2014). Development and migration of the *C. elegans* Q neuroblasts and their descendants. WormBook, 1-23. doi: 10.1895/wormbook.1.173.1

Middelkoop, T.C., Williams, L., Yang, P.T., Luchtenberg, J., Betist, M.C., Ji, N., van Oudenaarden, A., Kenyon, C., and Korswagen, H.C. (2012). The thrombospondin repeat containing protein MIG-21 controls a left-right asymmetric Wnt signaling response in migrating *C. elegans* neuroblasts. Dev Biol **361**, 338-348. doi: 10.1016/j.ydbio.2011.10.029

Moeller, M.J., Soofi, A., Braun, G.S., Li, X., Watzl, C., Kriz, W., and Holzman, L.B. (2004). Protocadherin FAT1 binds Ena/VASP proteins and is necessary for actin dynamics and cell polarization. EMBO J **23**, 3769-3779. doi: 10.1038/sj.emboj.7600380

Paix, A., Folkmann, A., Rasoloson, D., and Seydoux, G. (2015). High efficiency, homology-directed genome editing in *Caenorhabditis elegans* using CRISPR-Cas9 ribonucleoprotein complexes. Genetics **201**, 47-54. doi: 10.1534/genetics.115.179382

Pettitt, J. (2005). The cadherin superfamily. WormBook, 1-9. doi: 10.1895/wormbook.1.50.1

Pettitt, J., Wood, W.B., and Plasterk, R.H. (1996). *cdh-3*, a gene encoding a member of the cadherin superfamily, functions in epithelial cell morphogenesis in *Caenorhabditis elegans*. Development **122**, 4149-4157.

Quinn, C.C., and Wadsworth, W.G. (2008). Axon guidance: asymmetric signaling orients polarized outgrowth. Trends Cell Biol **18**, 597-603. doi: 10.1016/j.tcb.2008.09.005

Raj, A., van den Bogaard, P., Rifkin, S.A., van Oudenaarden, A., and Tyagi, S. (2008). Imaging individual mRNA molecules using multiple singly labeled probes. Nat Methods **5**, 877-879. doi: 10.1038/nmeth.1253

Salser, S.J., and Kenyon, C. (1992). Activation of a *C. elegans* Antennapedia homologue in migrating cells controls their direction of migration. Nature **355**, 255-258. doi: 10.1038/355255a0

Schmitz, C., Wacker, I., and Hutter, H. (2008). The Fat-like cadherin CDH-4 controls axon fasciculation, cell migration and hypodermis and pharynx development in *Caenorhabditis elegans*. Dev Biol **316**, 249-259. doi: 10.1016/j.ydbio.2008.01.024

Seetharaman, A., Selman, G., Puckrin, R., Barbier, L., Wong, E., D'Souza, S.A., and Roy, P.J. (2011). MADD-4 is a secreted cue required for midline-oriented guidance in *Caenorhabditis elegans*. Dev Cell **21**, 669-680. doi: 10.1016/j.devcel.2011.07.020

Shakir, M.A., Gill, J.S., and Lundquist, E.A. (2006). Interactions of UNC-34 Enabled with Rac GTPases and the NIK kinase MIG-15 in *Caenorhabditis elegans* axon pathfinding and neuronal migration. Genetics **172**, 893-913. doi: 10.1534/genetics.105.046359

Sulston, J.E., and Horvitz, H.R. (1977). Post-embryonic cell lineages of the nematode, *Caenorhabditis elegans*. Dev Biol **56**, 110-156.

Sulston, J.E., Schierenberg, E., White, J.G., and Thomson, J.N. (1983). The embryonic cell lineage of the nematode *Caenorhabditis elegans*. Dev Biol **100**, 64-119.

Sundararajan, L., and Lundquist, E.A. (2012). Transmembrane proteins UNC-40/DCC, PTP-3/LAR, and MIG-21 control anterior-posterior neuroblast migration with left-right functional asymmetry in *Caenorhabditis elegans*. Genetics **192**, 1373-1388. doi: 10.1534/genetics.112.145706

Sundararajan, L., Norris, M.L., Schoneich, S., Ackley, B.D., and Lundquist, E.A. (2014). The fat-like cadherin CDH-4 acts cell-non-autonomously in anterior-posterior neuroblast migration. Dev Biol **392**, 141-152. doi: 10.1016/j.ydbio.2014.06.009

Tang, X., and Wadsworth, W.G. (2014). SAX-3 (Robo) and UNC-40 (DCC) regulate a directional bias for axon guidance in response to multiple extracellular cues. PLoS One **9**, e110031. doi: 10.1371/journal.pone.0110031

Tanoue, T., and Takeichi, M. (2004). Mammalian Fat1 cadherin regulates actin dynamics and cell-cell contact. J Cell Biol **165**, 517-528. doi: 10.1083/jcb.200403006

Tessier-Lavigne, M., and Goodman, C.S. (1996). The molecular biology of axon guidance. Science **274**, 1123-1133. doi: 10.1126/science.274.5290.1123

Thevenaz, P., Ruttimann, U.E., and Unser, M. (1998). A pyramid approach to subpixel registration based on intensity. IEEE Trans Image Process **7**, 27-41. doi: 10.1109/83.650848

Tu, H., Pinan-Lucarre, B., Ji, T., Jospin, M., and Bessereau, J.L. (2015). *C. elegans* Punctin clusters GABA(A) receptors via Neuroligin binding and UNC-40/DCC recruitment. Neuron **86**, 1407-1419. doi: 10.1016/j.neuron.2015.05.013

Um, J.W., and Ko, J. (2013). LAR-RPTPs: synaptic adhesion molecules that shape synapse development. Trends Cell Biol **23**, 465-475. doi: 10.1016/j.tcb.2013.07.004

Wadsworth, W.G. (2002). Moving around in a worm: netrin UNC-6 and circumferential axon guidance in *C. elegans*. Trends Neurosci **25**, 423-429.

Wadsworth, W.G. (2018). A perspective on SOAL, a stochastic model of neuronal outgrowth. Dev Biol **443**, 92-101. doi: 10.1016/j.ydbio.2018.09.007

Wang, Z., Linden, L.M., Naegeli, K.M., Ziel, J.W., Chi, Q., Hagedorn, E.J., Savage, N.S., and Sherwood, D.R. (2014). UNC-6 (netrin) stabilizes oscillatory clustering of the UNC-40 (DCC) receptor to orient polarity. J Cell Biol **206**, 619-633. doi: 10.1083/jcb.201405026

Watanabe, K., Takebayashi, H., Bepari, A.K., Esumi, S., Yanagawa, Y., and Tamamaki, N. (2011). Dpy19l1, a multi-transmembrane protein, regulates the radial migration of glutamatergic neurons in the developing cerebral cortex. Development **138**, 4979-4990. doi: 10.1242/dev.068155

Whangbo, J., and Kenyon, C. (1999). A Wnt signaling system that specifies two patterns of cell migration in *C. elegans*. Mol Cell **4**, 851-858.

Wildwater, M., Sander, N., de Vreede, G., and van den Heuvel, S. (2011). Cell shape and Wnt signaling redundantly control the division axis of *C. elegans* epithelial stem cells. Development **138**, 4375-4385. doi: 10.1242/dev.066431

Yin, F., and Pan, D. (2007). Fat flies expanded the hippo pathway: a matter of size control. Sci STKE 2007, pe12. doi: 10.1126/stke.3802007pe12

Yu, T.W., Hao, J.C., Lim, W., Tessier-Lavigne, M., and Bargmann, C.I. (2002). Shared receptors in axon guidance: SAX-3/Robo signals via UNC-34/Enabled and a Netrin-independent UNC-40/DCC function. Nat Neurosci **5**, 1147-1154. doi: 10.1038/nn956

Zinovyeva, A.Y., Yamamoto, Y., Sawa, H., and Forrester, W.C. (2008). Complex network of Wnt signaling regulates neuronal migrations during *Caenorhabditis elegans* development. Genetics **179**, 1357-1371. doi: 10.1534/genetics.108.090290

Figures

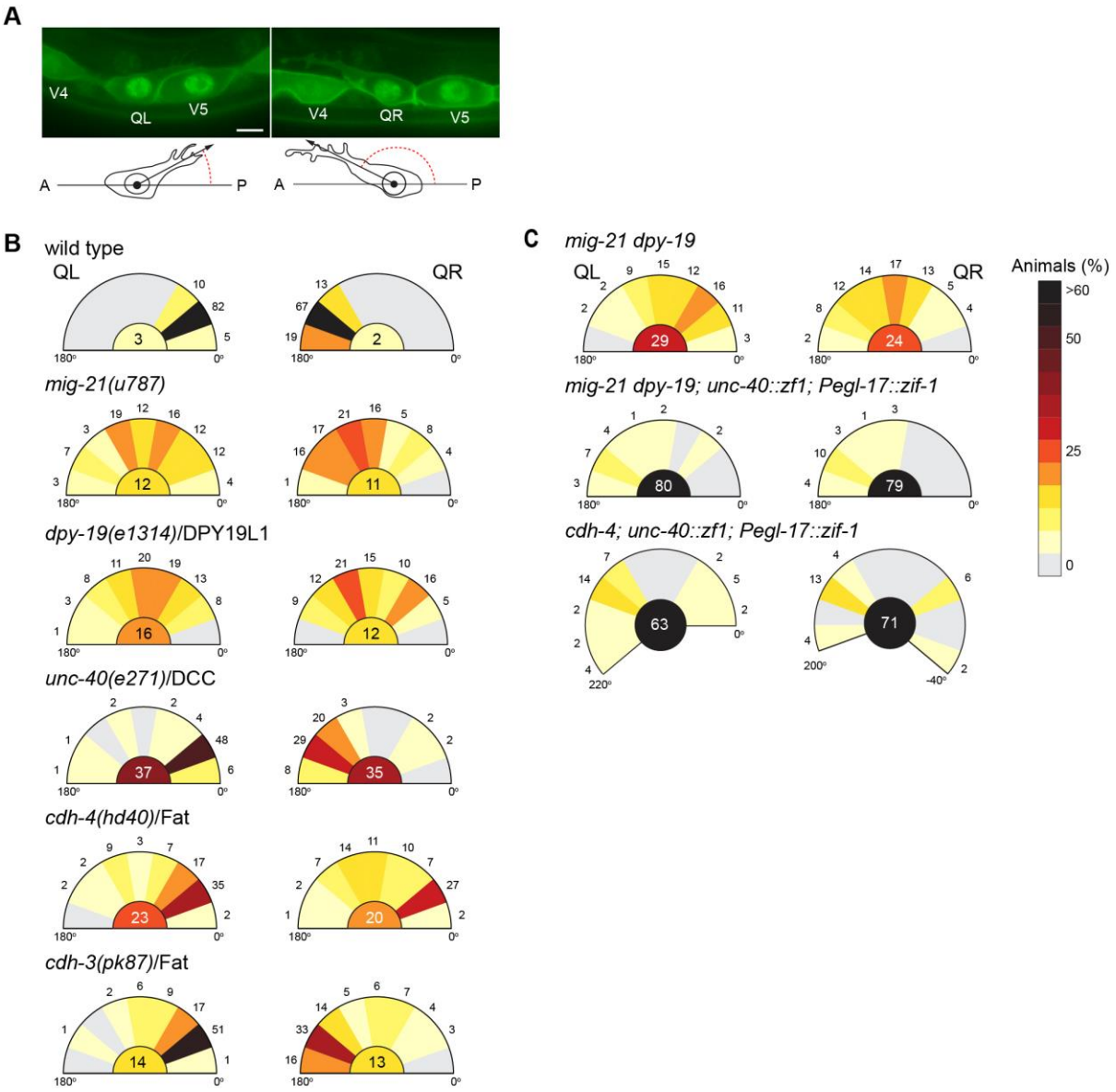

Figure 1. Polarization of the QL and QR neuroblasts. (**A**) Visualization of the Q neuroblast protrusion using membrane and nuclear localized GFP expressed in the Q neuroblasts and the seam (V) cells using the *heIs63* transgene (Wildwater et al., 2011). Anterior is left and dorsal is up. Schematic drawings illustrate the angle of the QL and QR protrusion relative to the anteroposterior body axis (0° is posterior and 180° anterior). Scale bar is 5 μm. (**B**, **C**) Quantification of protrusion formation and protrusion direction in wild type and polarity mutants 1-2 hours after hatching. Numbers and color coding represent percentages, n > 50. The percentage of cells that fail to form a major, lamellipodium-like protrusion is indicated in the center of the polar graphs. See Table S1 for statistical analysis of protrusion formation and direction.

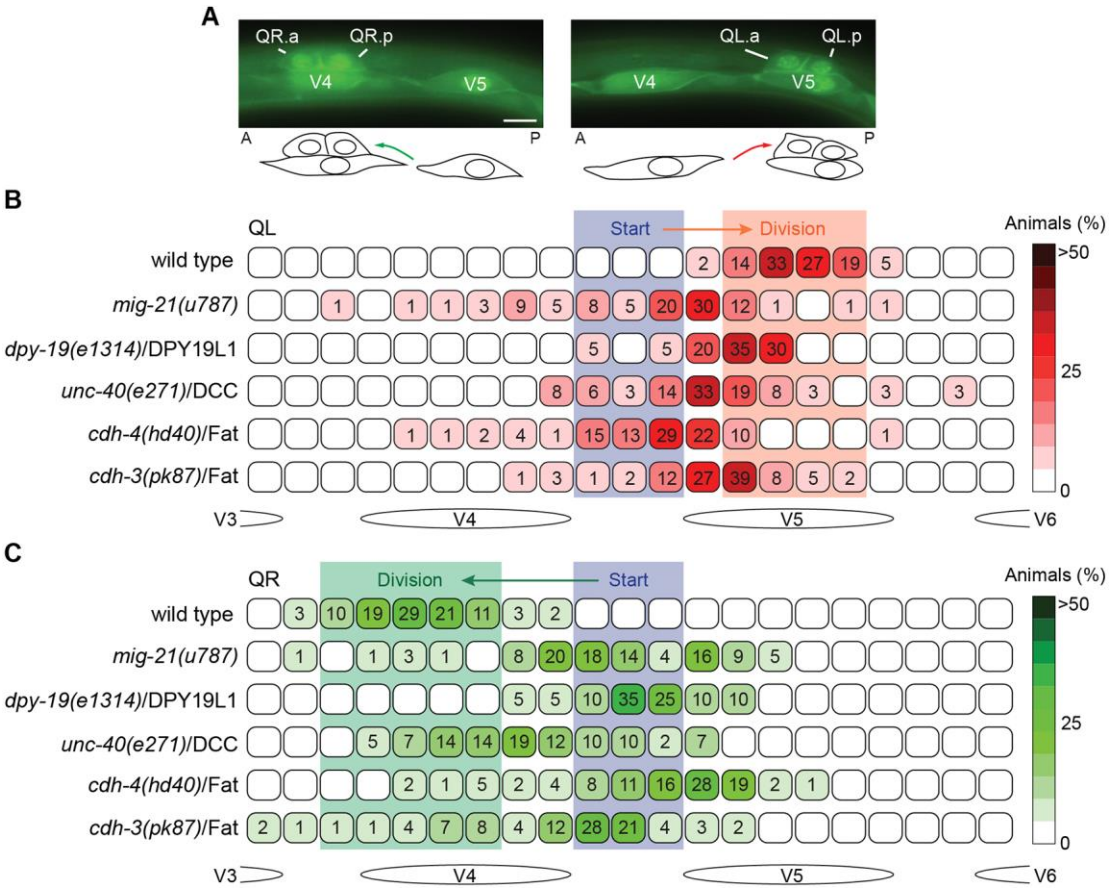

Figure 2. Migration of the QL and QR neuroblasts. (**A**) Visualization of the Q neuroblast division using membrane and nuclear localized GFP expressed in the Q neuroblasts and the seam (V) cells using the *heIs63* transgene. Anterior is left and dorsal is up. Schematic drawings illustrate the position of the Q cell division (the endpoint of the migration) relative to the seam cells V4 and V5. Scale bar is 5 μm. Quantification of QL (**B**) and QR (**C**) division position in wild type and polarity mutants relative to the seam cells V4 and V5. Blue area represents the starting point of the migration and the red and green boxes the point where QL and QR divide in wild type animals. Numbers and color coding represent percentages, n > 20. See Table S1 for statistical analysis of Q division position.

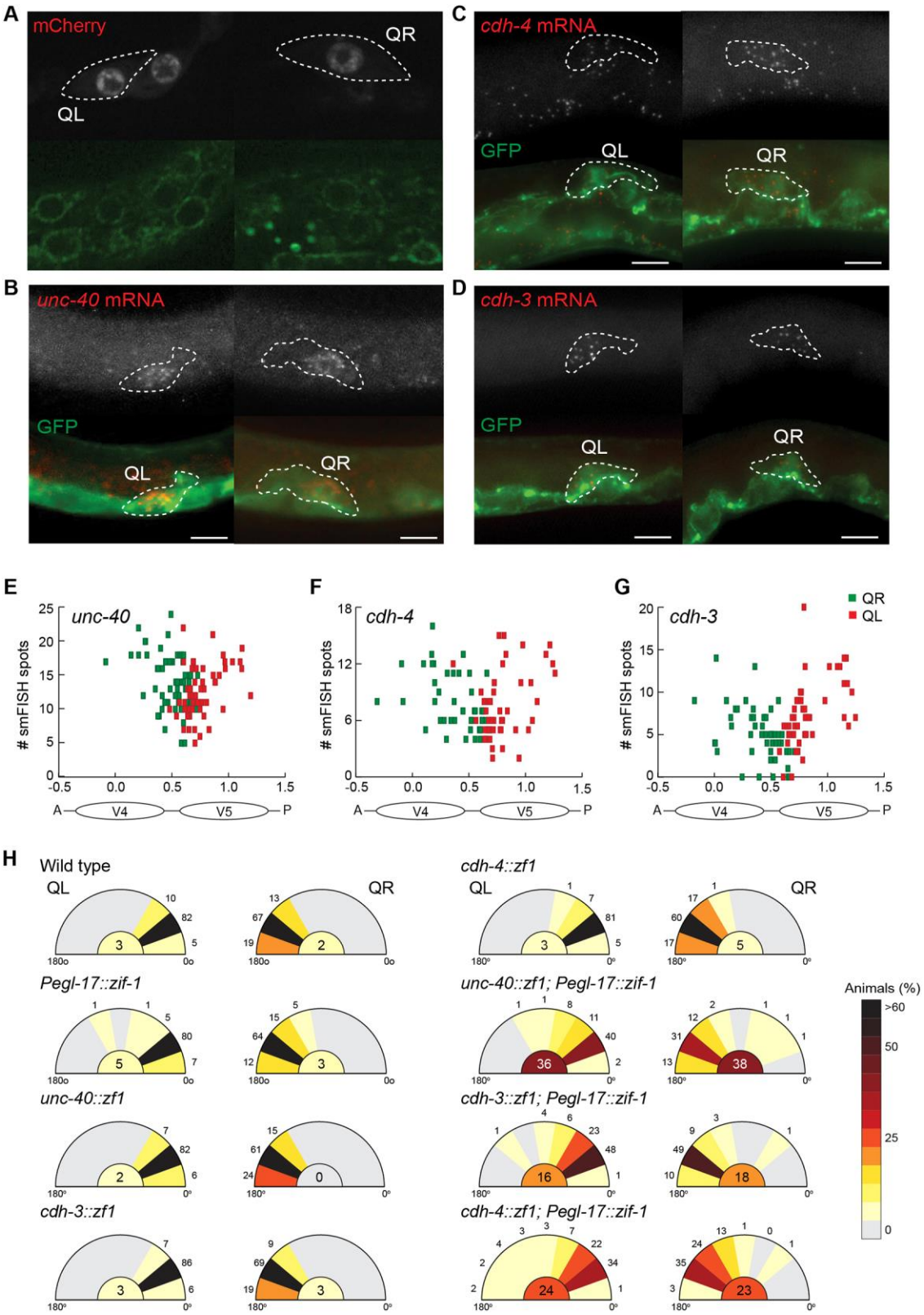

Figure 3. Expression and site of action of Q neuroblast polarity genes. (**A**) Representative images of endogenous DPY-19::GFP localization in the Q neuroblast and the surrounding seam cells and hypodermal syncytium. Arrows indicate localization of DPY-19::GFP at the nuclear periphery of QL and QR. The membrane and nucleus of the Q

neuroblasts and the seam (V) cells are labeled with mCherry (*huIs166*). The outline of the Q neuroblast is indicated with a dashed line. (**B**, **C**, **D**) Single molecule mRNA FISH (smFISH) of *unc-40*, *cdh-4* and *cdh-3* in polarizing Q neuroblasts 1-2 hours after hatching. The membrane and nucleus of the Q neuroblasts and the seam (V) cells are labeled with GFP (*heIs63*). The outline of the Q neuroblast is indicated with a dashed line. Anterior is left and dorsal is up. Scale bars are 5 μm. (**E**, **F**, **G**) Quantification of smFISH spots in the QL (green) and QR (red) neuroblasts during polarization and migration (0-5 hours after hatching). The position of each cell is plotted relative to the seam cells V4 and V5, with both cells starting at a position between V4 and V5 (around 0.5) and migrating either towards the anterior (QR, <0.5) or posterior (QL, >0.5). The expression of *unc-40*, *cdh-4* and *cdh-3* positively correlates with migration distance (*unc-40* QL: $r = 0.4081$, $p < 0.0022$, QR: $r = -0.2838$, $p < 0.0324$, *cdh-3* QL: Spearman $r = 0.5765$, $p < 0.0001$, QR: Spearman $r = -0.4838$, $p < 0.0004$, *cdh-4* QL: Spearman $r = 0.3176$, $p < 0.03$, QR: Spearman $r = -0.5070$, $p < 0.0004$). (**H**) Quantification of protrusion formation and protrusion direction in wild type and animals with Q lineage specific depletion (*Pegl-17::ZIF-1*) of *unc-40::ZF1*, *cdh-4::ZF1* and *cdh-3::ZF1* 1-2 hours after hatching. Numbers and color coding represent percentages, $n > 61$. The percentage of cells that fail to form a major, lamellipodium-like protrusion is indicated in the center of the polar graphs. See Table S1 for statistical analysis of protrusion formation and direction.

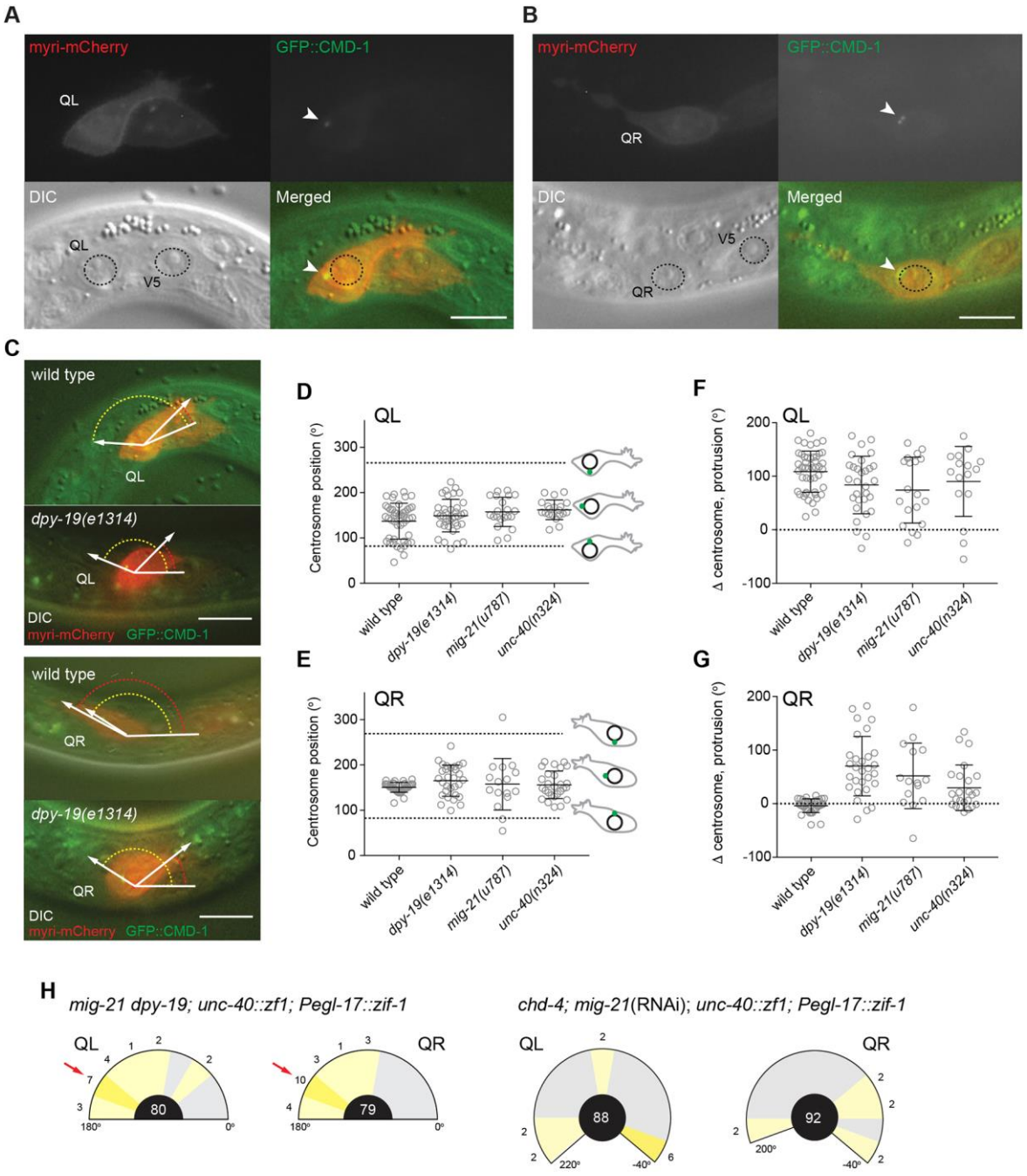

Figure 4. Centrosome position and role of *cdh-4* in anterior ground polarity. (**A**, **B**) Centrosome position in QL and QR. Localization of the centrosome marker GFP::CMD-1 and myristoylated mCherry (*caIs22*) (Chai et al., 2012) at 2 hours after hatching. The nuclei of the Q neuroblast and seam cell V5 are indicated by a dashed line, the centrosome by an arrow. Scale bars are 5 μm. (**C**) Examples of protrusion (red dashed line) and centrosome (yellow dashed line) angles relative to the anteroposterior body axis (defined by a line between the centers of the Q and V5 nuclei) in wild type and *dpy-19(e1314)* mutants. Scale bars are 10 μm. (**D**, **E**) Angle of the centrosome relative to the anteroposterior axis in QL and QR. Comparing the variance of QL and QR in all conditions shows that only in wild type the

variance is unequal; F-value = 28.8, Pr(>F) < 0.0001 (Levene's test for homogeneity of variance), n > 14. (**F**, **G**) Difference in the angle of the centrosome and the main protrusion in QL and QR. (**H**) Quantification of protrusion formation and protrusion direction at 1-2 hours after hatching. The anterior bias in protrusion direction in the absence of *mig-21*, *dpy-19* and *unc-40* is indicated by red arrows. Numbers and color coding represent percentages, n > 50. The percentage of cells that fail to form a major, lamellipodium-like protrusion is indicated in the center of the polar graphs. See Table S1 for statistical analysis of protrusion formation and direction.

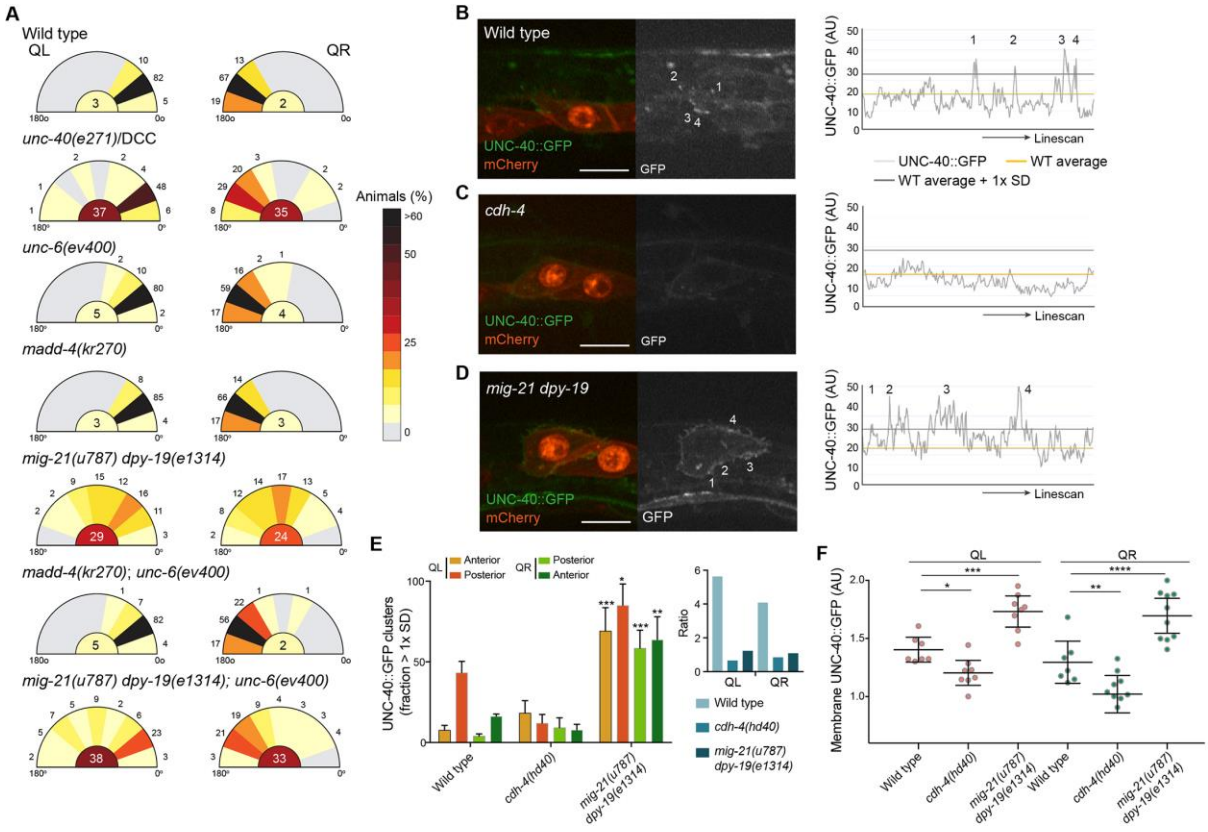

Figure 5. Ligand-independent clustering of UNC-40/DCC at the leading edge of the polarizing Q neuroblast. (**A**) Quantification of protrusion formation and protrusion direction 1-2 hours after hatching. Numbers and color coding represent percentages, n > 61. The percentage of cells that fail to form a major, lamellipodium-like protrusion is indicated in the center of the polar graphs. See Table S1 for statistical analysis of protrusion formation and direction. (**B**, **C**, **D**) Endogenous UNC-40::GFP localization in wild type, *cdh-4(hd40)* and *mig-21 (u787) dpy-19(e1314)* mutants. The plasma membrane and nucleus of the QR neuroblast and seam (V) cells are labeled with mCherry (*huIs166*). GFP localization at the plasma membrane was quantified by line-scan (counter clockwise, starting from the site of contact between the Q neuroblast and seam cell V4). Numbers indicate UNC-40::GFP punctae (defined as average + 1x SD). Anterior is left and dorsal is up. Scale bars are 10 μm. (**E**) Quantification of plasma membrane UNC-40::GFP clusters (defined as fraction of membrane with fluorescence above the average + 1x SD in wild type) at the anterior versus posterior side of the QL and QR neuroblasts. *p < 0.05, **p < 0.01, ***p < 0.005 (Tukey's multiple comparisons test), n > 7. (**F**) Membrane localization of UNC-40::GFP (normalized mean fluorescence at the membrane divided by normalized mean fluorescence of the cytoplasm). *p < 0.05, **p < 0.01, ***p < 0.005, ****p < 0.0005 (Holm-Sidak's multiple comparisons test), n > 7.

Supplemental Figures

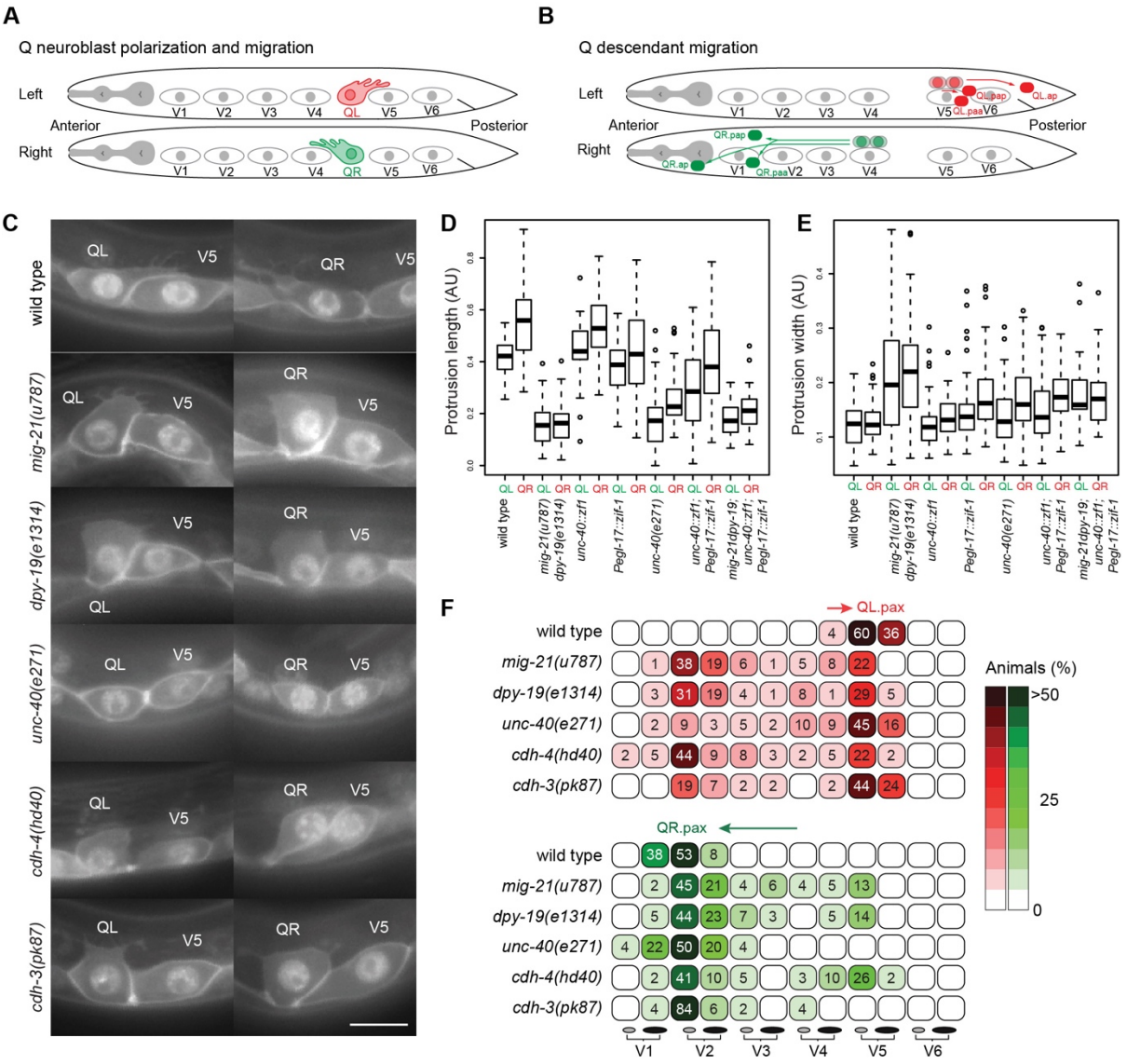

Figure S1. Polarization and migration of the Q neuroblasts and their descendants. (**A**) Schematic overview of the initial polarization and migration of the QL and QR neuroblasts. QL forms a lamellipodium-like protrusion towards the posterior and QR towards the anterior. After stable protrusion formation, the QL and QR cell bodies migrate to positions dorsal to V5 and V4 respectively. (**B**) After migration, QL and QR undergo an identical pattern of division, generating three neurons and two cells that undergo apoptosis. On the left side, the QL.p descendants remain close to the position of QL division, while the QL.a descendant QL.ap migrates to a position in the tail. On the right side, both the QR.a and QR.p descendants migrate anteriorly. (**C**) Representative images of Q neuroblast polarization in wild type and polarity mutants (1-2 hours after hatching). Anterior is left and dorsal is up. Scale bar is 10 μm. Quantification of protrusion length (**D**) and protrusion width (**E**) in wild type and polarity mutants (1-2 hours after hatching). (**F**) Final position of the Q. descendants Q.paa and Q.pap (Q.pax) relative to the seam cells. Arrows indicate direction of migration. Numbers and color coding represent percentages, n > 45. See Table S1 for statistical analysis of Q.pax position.

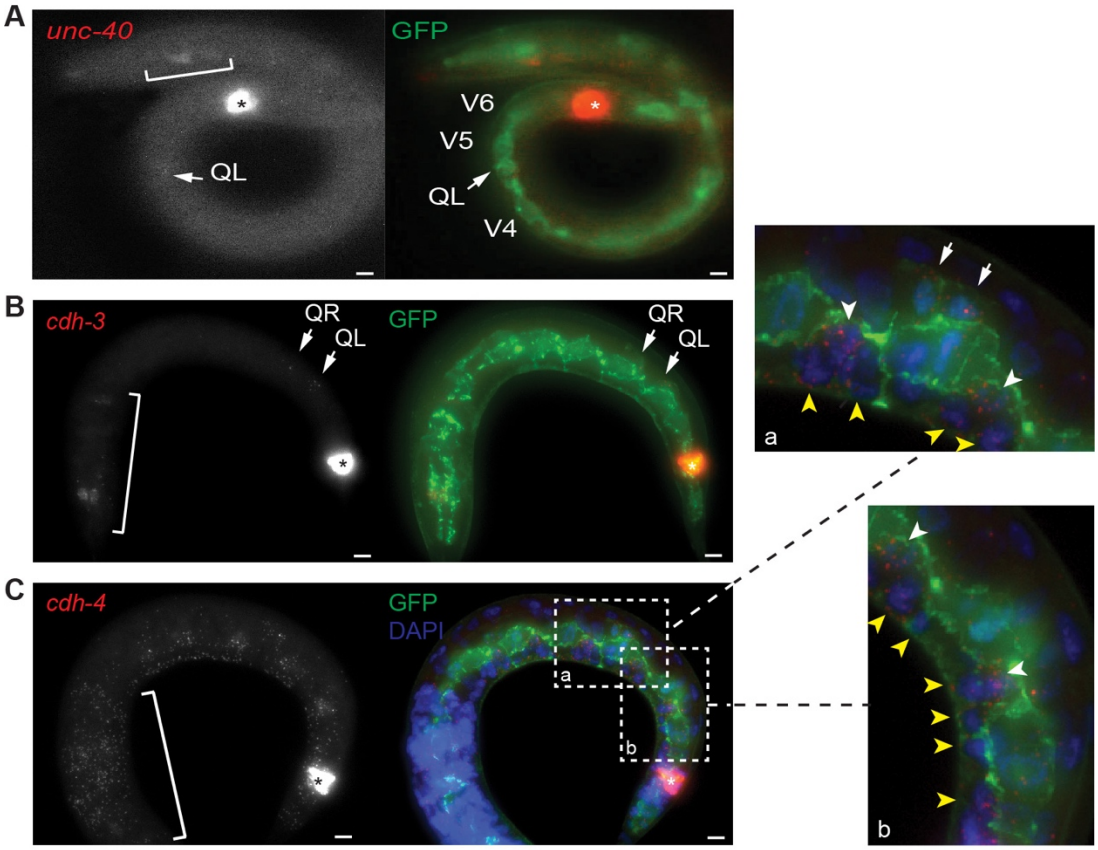

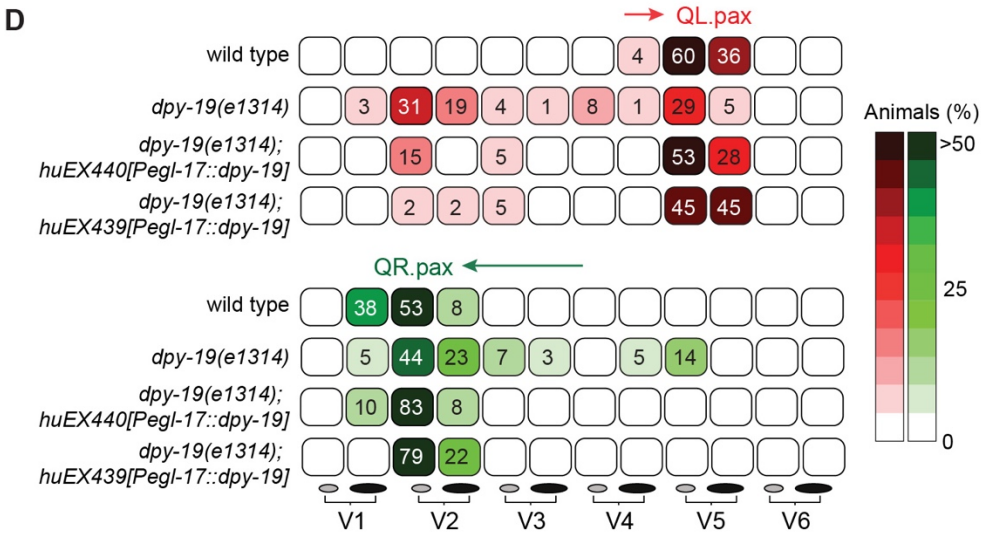

Figure S2. Expression patterns of *unc-40*, *cdh-3* and *cdh-4*. (A, B, C) smFISH at 1-2 hours after hatching. The Q neuroblasts and seam (V) cells are labeled with GFP (heIs63). Arrows indicate the Q neuroblasts, brackets expression in the head region and asterisk expression of the co-injection marker. (**C a**, **b**) Higher magnification images showing expression in the Q neuroblasts (white arrows), juvenile ventral cord neurons (yellow arrowheads) and P cells (white arrowheads). Anterior is left and dorsal is up. Scale bars are 5 μm. (**D**) Final position of the Q. descendants Q.paa and Q.pap (Q.pax) relative to the seam cells. Arrows indicate direction of migration. Numbers and color coding represent percentages, n > 40. See Table S1 for statistical analysis of Q.pax position.

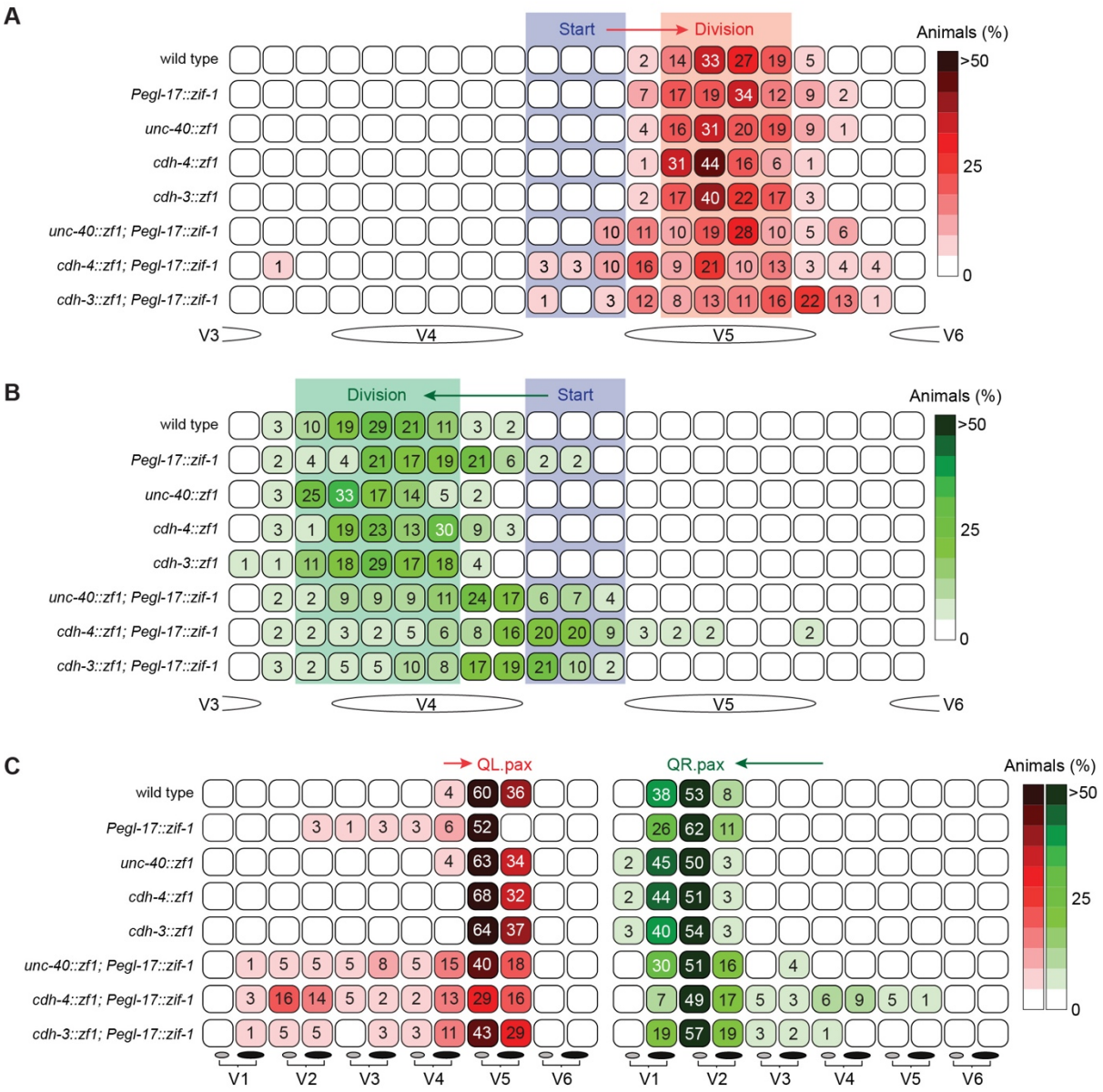

Figure S3. Q lineage specific depletion of UNC-40, CDH-4 and CDH-3. Quantification of QL (**A**) and QR (**B**) division position in animals in which *unc-40*, *cdh-4* and *cdh-3* are endogenously tagged with the *zf-1* sequence, and in which ZIF-1 is specifically expressed in the Q neuroblast lineage (*Pegl-17::zif-1*). Blue area represents the starting point of the migration and the red and green boxes the point where QL and QR divide in wild type animals. Numbers and color coding represent percentages, n > 45. (**C**) Final position of the Q. descendants Q.paa and Q.pap (Q.pax) relative to the seam cells. Arrows indicate direction of migration. Numbers and color coding represent percentages, n > 25. See Table S1 for statistical analysis of Q division position and Q.pax position.

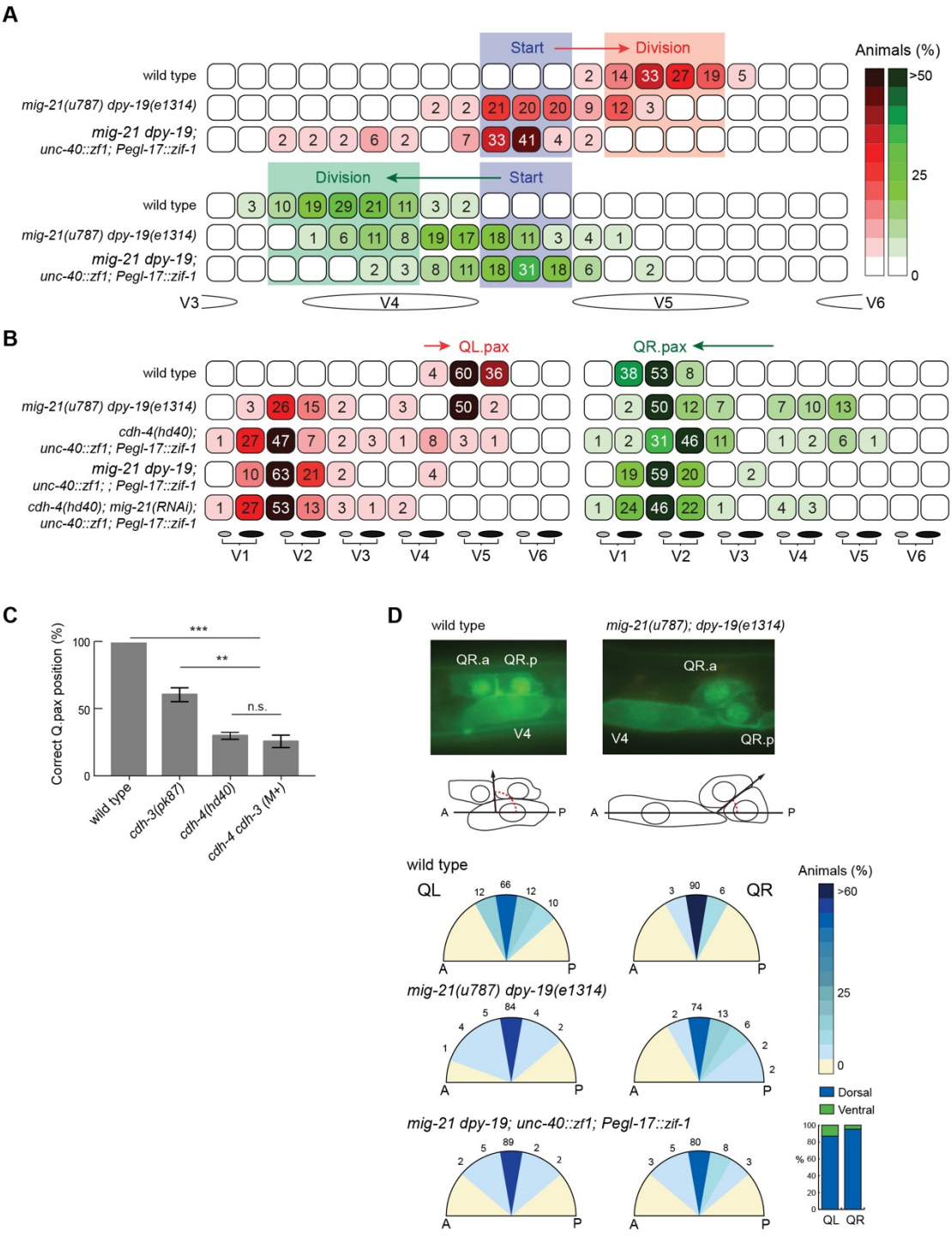

Figure S4. Polarization and migration of the Q neuroblasts and their descendants in the combined absence of polarity pathways. (**A**) Quantification of QL and QR division position in *mig-21(u787) dpy-19(e1314)* double mutants combined with Q lineage specific depletion of UNC-40 (*unc-40::zf-1; Pegl-17::zif-1*). Blue area represents the starting point of the migration and the red and green boxes the point where QL and QR divide in wild type animals. Numbers and color coding represent percentages, n > 50. (**B**) Final position of the Q. descendants Q.paa and Q.pap (Q.pax) relative to the seam cells. *mig-21* was knocked down by feeding RNAi. Arrows indicate direction of migration. Numbers and color coding represent percentages, n > 50. See Table S1 for statistical analysis of Q division position and Q.pax position. (**C**) Quantification of Q.pax position in *cdh-3(pk87)* and *cdh-4(hd40)* single and

maternally rescued (M+) double mutants. Numbers represent mean ± SD from three independent experiments (each n > 50). **p < 0.003, ***p < 0.0004, n.s., not significant (Student's t-test). (**D**) Quantification of the division plane of QL and QR. In wild type, a line through the point of contact between Q.a and Q.p is at a 90^{o} angle with the anteroposterior axis. In *mig-21(u787) dpy-19(e1314)* double mutants, the orientation of the Q division is more variable. Numbers and color coding represent percentages, n > 50. When UNC-40 is depleted (*unc-40::zf-1; Pegl-17::zif-1*) in *mig-21 dpy-19* double mutants, the Q neuroblasts occasionally divide ventral to the seam cells (bar diagram).

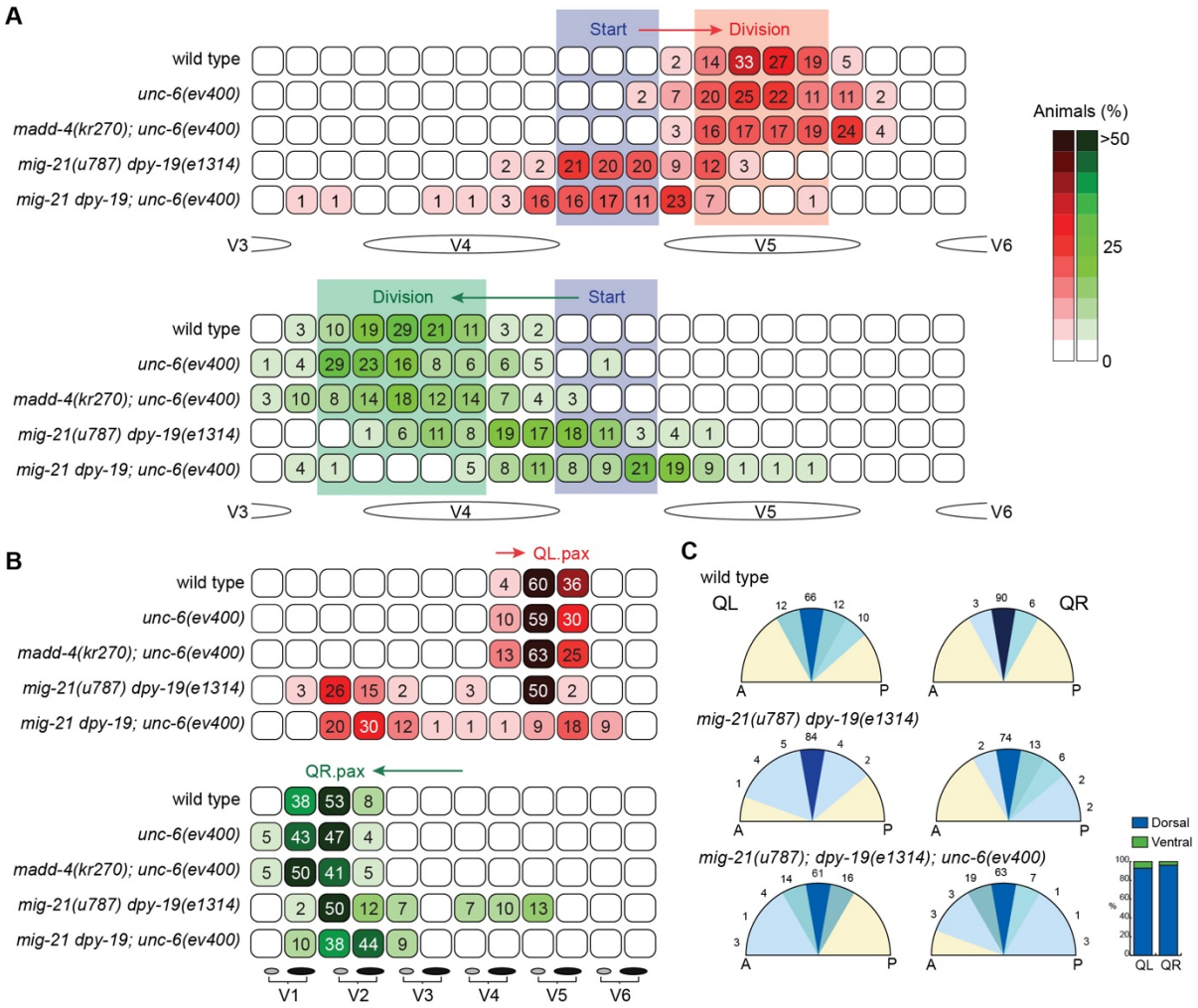

Figure S5. Polarization and migration of the Q neuroblasts and their descendants in the absence of the UNC-40 ligands UNC-6 and MADD-4. (**A**) Quantification of QL and QR division position. Blue area represents the starting point of the migration and the red and green boxes the point where QL and QR divide in wild type animals. Numbers and color coding represent percentages, n > 33. (**B**) Final position of the Q. descendants Q.paa and Q.pap (Q.pax) relative to the seam cells. Arrows indicate direction of migration. Numbers and color coding represent percentages, n > 47. See Table S1 for statistical analysis of Q division position and Q.pax position. (**C**) Quantification of the division plane of QL and QR. In wild type, a line through the point of contact between Q.a and Q.p is at a 90° angle with the anteroposterior axis. In *mig-21(u787) dpy-19(e1314)* double mutants and *mig-21 dpy-19*; *unc-6(ev400)* triple mutants, the orientation of the Q division is more variable. Numbers and color coding represent percentages, n > 50. In *mig-21 dpy-19*; *unc-6* triple mutants, the Q neuroblasts occasionally divide ventral to the seam cells (bar diagram).

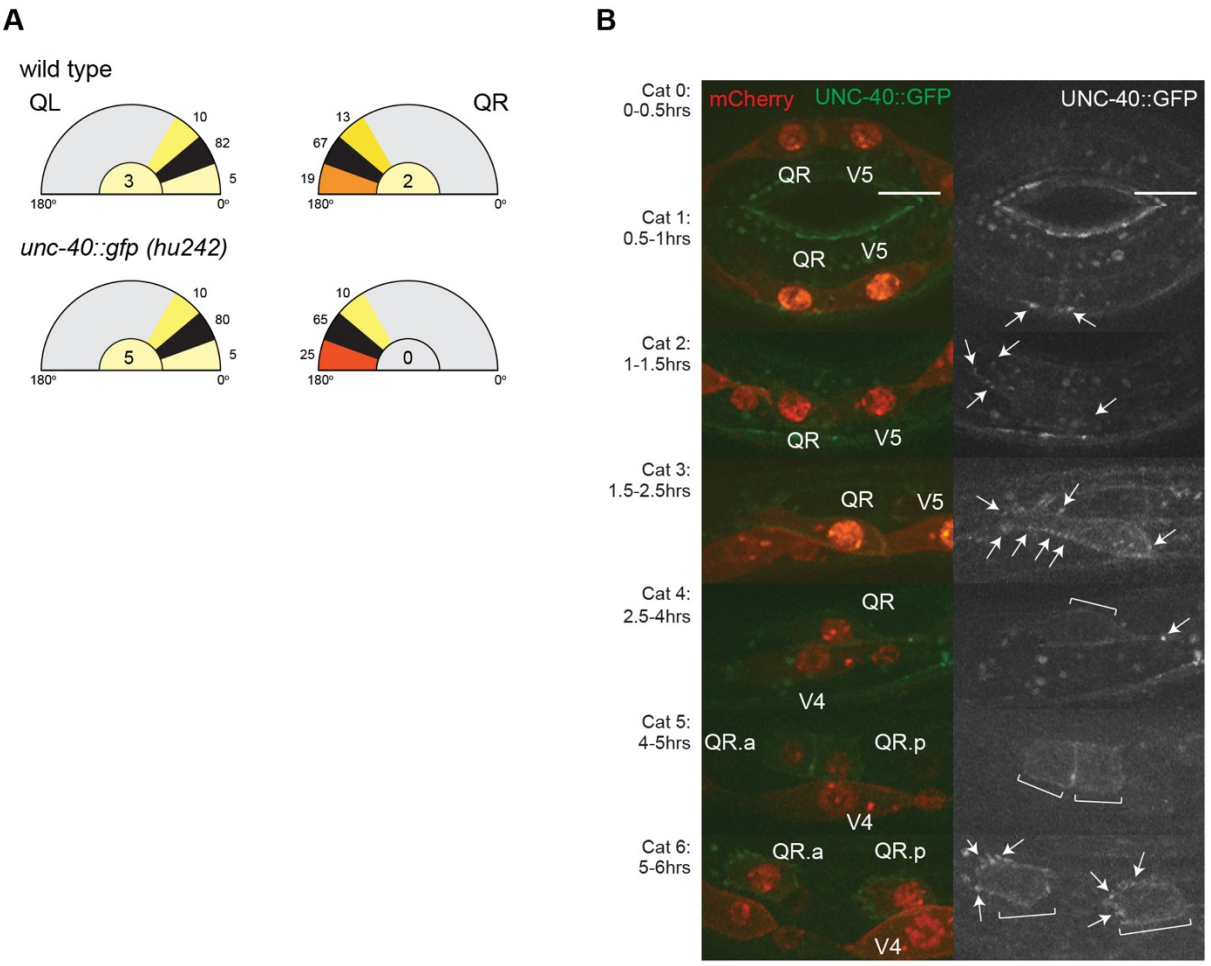

Figure S6. Endogenous UNC-40::GFP expression. (**A**) Quantification of protrusion formation and protrusion direction in wild type and *unc-40::gfp(hu242)* at 1-2 hours after hatching. Numbers and color coding represent percentages, n > 20. The percentage of cells that fail to form a major protrusion is indicated in the center of the polar graphs. See Table S1 for statistical analysis of protrusion formation and direction. (**B**) Representative images of UNC-40::GFP localization during polarization, migration and division (indicated by category and time after hatching). The plasma membrane and nucleus of the Q neuroblasts and seam (V) cells are labeled with mCherry (*huIs166*). UNC-40::GFP punctae are indicated by arrows. Brackets indicate diffuse UNC-40::GFP localization at the plasma membrane. Anterior is left and dorsal up. Scale bar is 10 μm.

Supplemental Tables

Table S1.1 Statistical analysis of Q polarization.
Click here to Download Table S1.1

Table S1.2 Statistical analysis of Q position of division
Click here to Download Table S1.2

Table S1.3 Statistical analysis of Q.pax position
Click here to Download Table S1.3

Table S2. Transgenic mosaic analysis to determine the site of action of *dpy-19*

Genotype	Body shape	Percentage Q.pax migration defect*
dpy-19(e1314); huEx439[Pegl-17::dpy-19]		
Transgenic	Dpy	35.3 ± 5.0**
Transgenic	WT	21.3 ± 7.0
Non-transgenic siblings	Dpy	59.0 ± 5.6
dpy-19(e1314); huEx440[Pegl-17::dpy-19]		
Transgenic	Dpy	20.3 ± 4.0**
Transgenic	WT	7.90 ± 0.1
Non-transgenic siblings	Dpy	66.9 ± 8.2

Expression of wild type *dpy-19* in the Q neuroblast lineage of *dpy-19(e1314)* mutants rescues Q.pax migration (Fig. S2). However, in some of the transgenic animals, the Dpy phenotype is rescued as well. This indicates that despite the specificity of the *egl-17* promoter for the Q cell lineage, these transgenes may display a low level of *dpy-19* expression in the hypodermis. To circumvent this problem, we made use of the fact that extra-chromosomal transgenes are frequently lost during somatic cell divisions, leading to mosaic expression of the transgene. Using this approach, we found that transgenic mosaics that remain Dpy still show significant rescue of Q.pax migration, supporting our conclusion that *dpy-19* functions cell autonomously in the Q cell lineage. * mean ± SD. **t-test siblings versus Dpy: p=0.0056 and 0.0034 for *huEx439* and *huEx440*, respectively.

Table S3. Primers and oligonucleotides

	Sequence
***dpy-19* expression construct**	
dpy-19 FW	GGGGACAAGTTTGTACAAAAAAGCAGGCTATGGCAAAGAAACCCAAGAATTC
dpy-19 RV	GGGGACCACTTTGTACAAGAAAGCTGGGTTTCAGATTTTCAAAACAATATAAT TCCT
Guide RNAs zf1 tagging	
unc-40	CCTCCTATTGCGAGATGTCTTGATGGATAAGTAATAATAATCGTTTAAGAGCT ATGCTGG
cdh-4	CCTCCTATTGCGAGATGTCTTGGTGAATTAAAGAAATACTGAGTTTAAGAGCT ATGCTGG
cdh-3	CCTCCTATTGCGAGATGTCTTGTAGAGACGGGCACATTAATAGTTTAAGAGC TATGCTGG
ssODN zf1 repair templates	
unc-40	ACAACAATTACAGCACAATTTGCATTTTGAGACGAGTATGGATAAGACAGAAT ACAAAACGCGACTTTGTGATGCGTTCCGCCGTGAAGGATACTGCCCGTACAA CGACAATTGCACATATGCTCACGGACAAGATGAGCTGAGAGTTCCGAGATAA TAATAATCTAGTATTTTTTTGATAATTTGAATTATTAATTTTG
cdh-4	TTTGATGATATAGACGAAGAAGTCAACATTCACATCTCTACAGAATACAAAAC GCGACTTTGTGATGCGTTCCGCCGTGAAGGATACTGCCCGTACAACGACAA TTGCACATATGCTCACGGACAAGATGAGCTGAGAGTTCCGAGATAATAACAT TCAGTATTTCTTTAATTCACAATTTCTCAA
cdh-3	CTGCACCATCTTACCGTAGAGACGGGCACATTAATATAGCTTACTTAACAGA ATACAAAACGCGACTTTGTGATGCGTTCCGCCGTGAAGGATACTGCCCGTAC AACGACAATTGCACATATGCTCACGGACAAGATGAGCTGAGAGTTCCGAGAT AGAGATATTTTATTTTCATCATTTTCGATTCATTTTTACGGGTT
SEC cassette cloning	
unc-40 sgRNA	GTAATACGACTCACTATAGGATGGATAAGTAATAATAATCGTTTTAGAGCTAG AAATAGC
dpy-19 sgRNA	GTAATACGACTCACTATAGGAAATAGTTTATAATGCTAATGTTTTAGAGCTAG AAATAGC
reverse sgRNA primer	AAAAGCACCGACTCGGTGC
HA 1 *dpy-19* FW	ACGTTGTAAAACGACGGCCAGTCGCCGGCAACAGTTGAATGTCAAGGGAGA A
HA 1 *dpy-19* RV	CATCGATGCTCCTGAGGCTCCCGATGCTCCGATTTTCAAAACAATATAATTTC TATTAGC
HA 2 *dpy-19* FW	CGTGATTACAAGGATGACGATGACAAGAGATGATTTTTTTCTATTTTGTTTTTA AATTTA
HA 1 *dpy-19* RV	GGAAACAGCTATGACCATGTTATCGATTTCTTTAGGCGGAAACCTCAGAC
HA 1 *unc-40* FW	ACGTTGTAAAACGACGGCCAGTCGCCGGCACGGTGGACGGCAAGTTCCAGT TGGAAGAGC
HA 1 *unc-40* RV	CATCGATGCTCCTGAGGCTCCCGATGCTCCCTTATCCATACTCGTCTCAAAA TGCAAATT
HA 2 *unc-40* FW	CGTGATTACAAGGATGACGATGACAAGAGATAATAATAATCTGGTATTTTTTT GATAATT
HA 1 *unc-40* RV	GGAAACAGCTATGACCATGTTATCGATTTCGGATGTTAATCTGACAACTCTCA TCTCC

Supplemental Movies

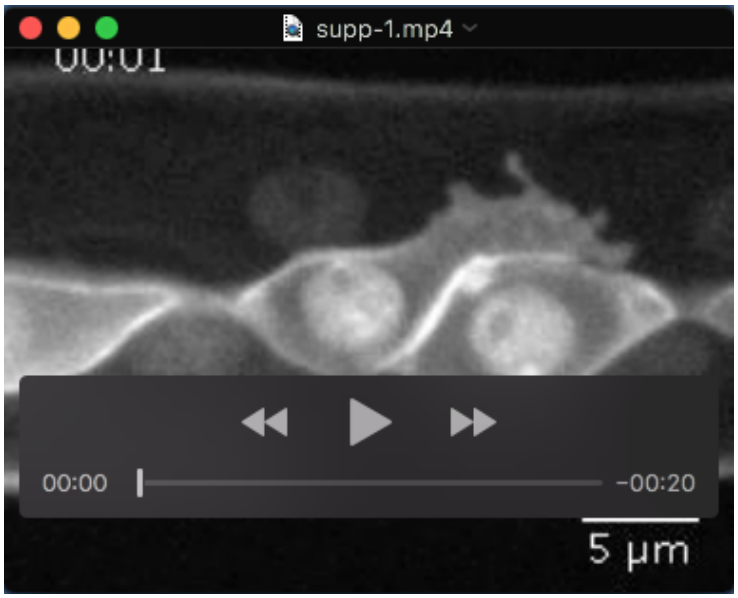

Movie 1. Live time-lapse confocal imaging of wild type animals expressing plasma membrane and nuclear localized GFP in QL and the seam cells (transgene *heIs63*). Anterior is left. Images were acquired every minute for a total duration of 1.5 hours. Movies are played at 5 frames per second.

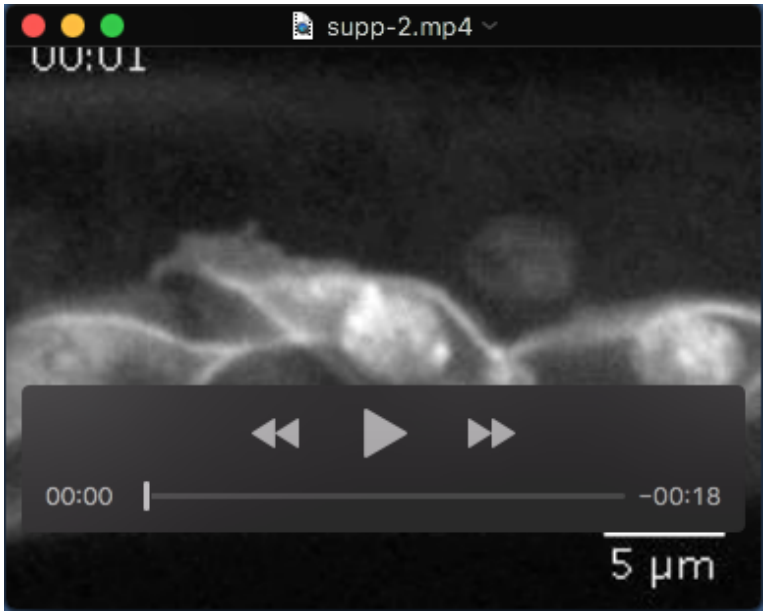

Movie 2. Live time-lapse confocal imaging of wild type animals expressing plasma membrane and nuclear localized GFP in QR and the seam cells (transgene *heIs63*). Anterior is left. Images were acquired every minute for a total duration of 1.5 hours. Movies are played at 5 frames per second.

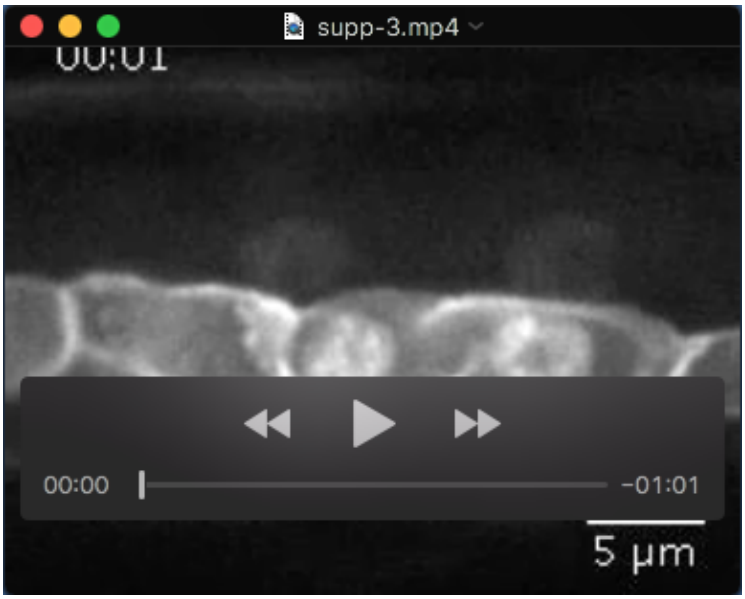

Movie 3. Live time-lapse confocal imaging of *cdh-4(hd40)* animals expressing plasma membrane and nuclear localized GFP in QL and the seam cells (transgene *heIs63*). A nterior is left. Images were acquired every minute for a total duration of 5 hours. Movies are played at 5 frames per second.

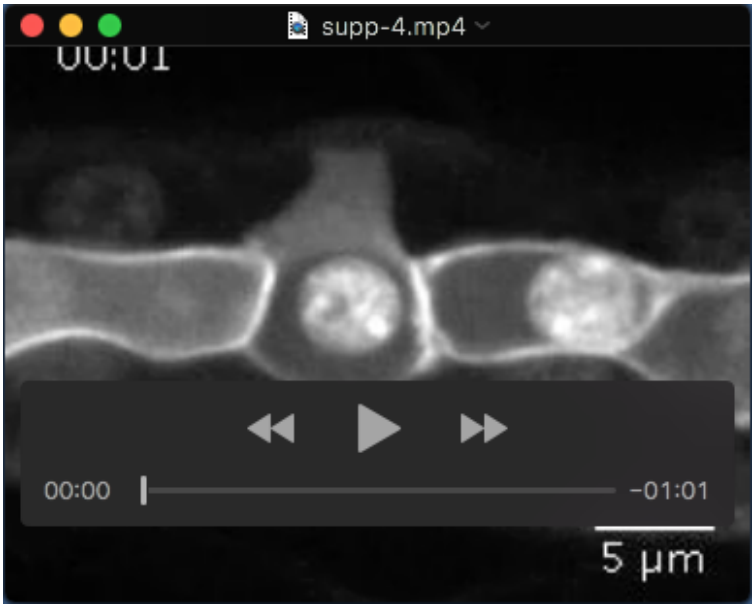

Movie 4. Live time-lapse confocal imaging of *cdh-4(hd40)* animals expressing plasma membrane and nuclear localized GFP in QR and the seam cells (transgene *heIs63*). Anterior is left. Images were acquired every minute for a total duration of 5 hours. Movies are played at 5 frames per second.

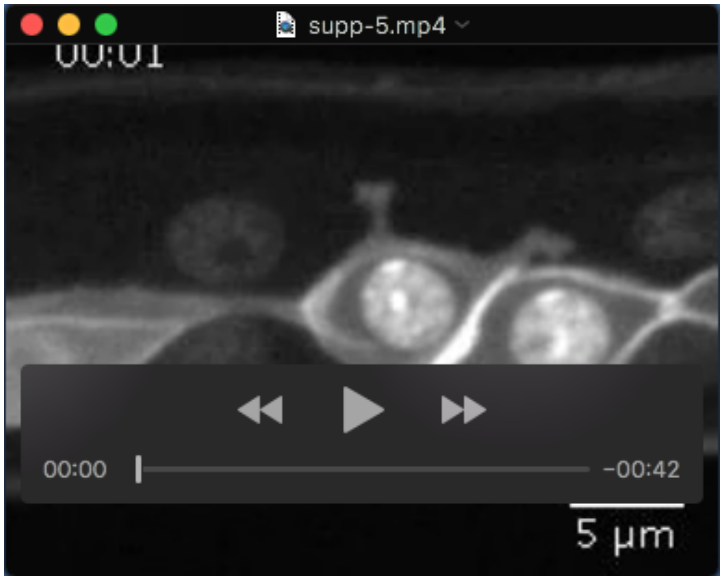

Movie 5. Live time-lapse confocal imaging of *cdh-3(pk87)* animals expressing plasma membrane and nuclear localized GFP in QL and the seam cells (transgene *heIs63*). Anterior is left. Images were acquired every minute for a total duration of 3.5 hours. Movies are played at 5 frame s per second.

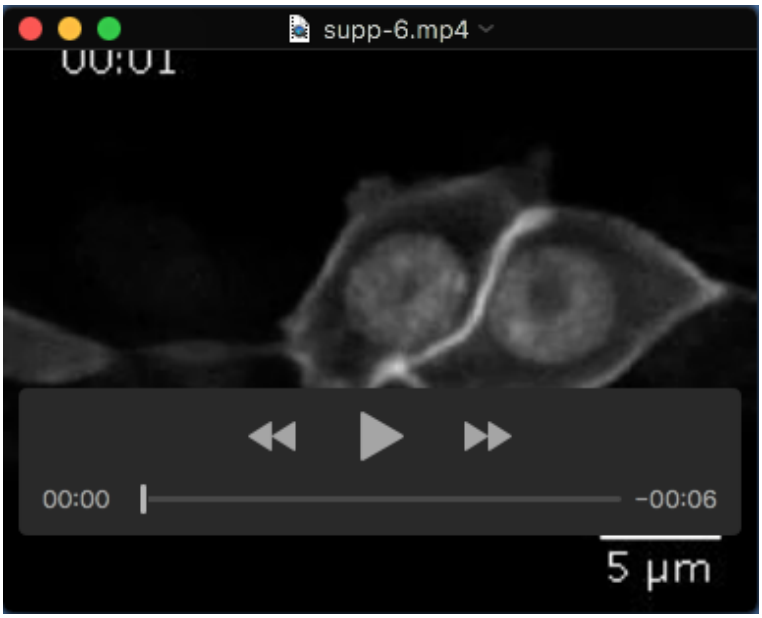

Movie 6. Live time-lapse confocal imaging of *unc-40(e271)* animals expressing plasma membrane and nuclear localized GFP in QL and the seam cells (transgene *heIs63*). Anterior is left. Ima ges were acquired every minute for a total duration of 1 hour. Movies are played at 5 frames per second.

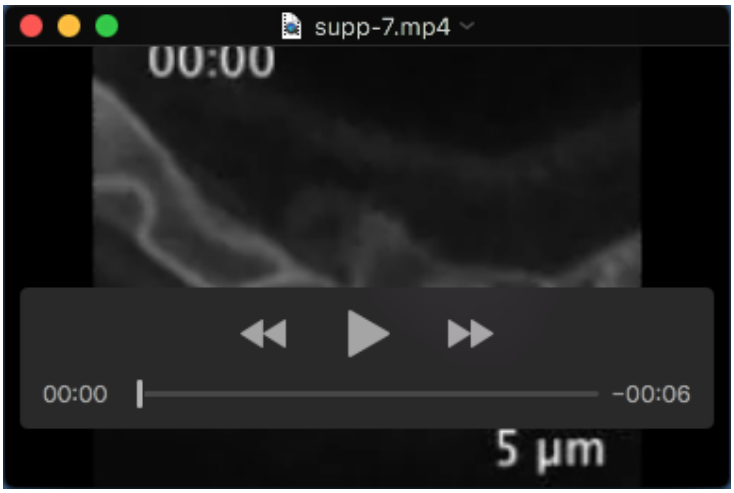

Movie 7. Live time-lapse confocal imaging of *unc-40(hu226[unc-40::zf1]); mig-21(u787) dpy-19(e1314); huIs181[Pegl-17::zif-1-SL2-mcherry; Pmyo-2::mcherry]* animals expressing plasma membrane and nuclear localized GFP in QL and the seam cells (transgene *heIs63*). Anterior is left. Images were acquired every 10 minutes for a total duration of 3 hours. Movies are played at 3 frames per second.

Movie 8. Live time-lapse confocal imaging of *unc-40(hu226[unc-40::zf1]); mig-21(u787) dpy-19(e1314); huIs181[Pegl-17::zif-1-SL2-mcherry; Pmyo-2::mcherry]* animals expressing plasma membrane and nuclear localized GFP in QR and the seam cells (transgene *heIs63*). Anterior is left. Images were acquired every 10 minutes for a total duration over 4.5 hours. Movies are played at 3 frames per second.

Supplemental Figures

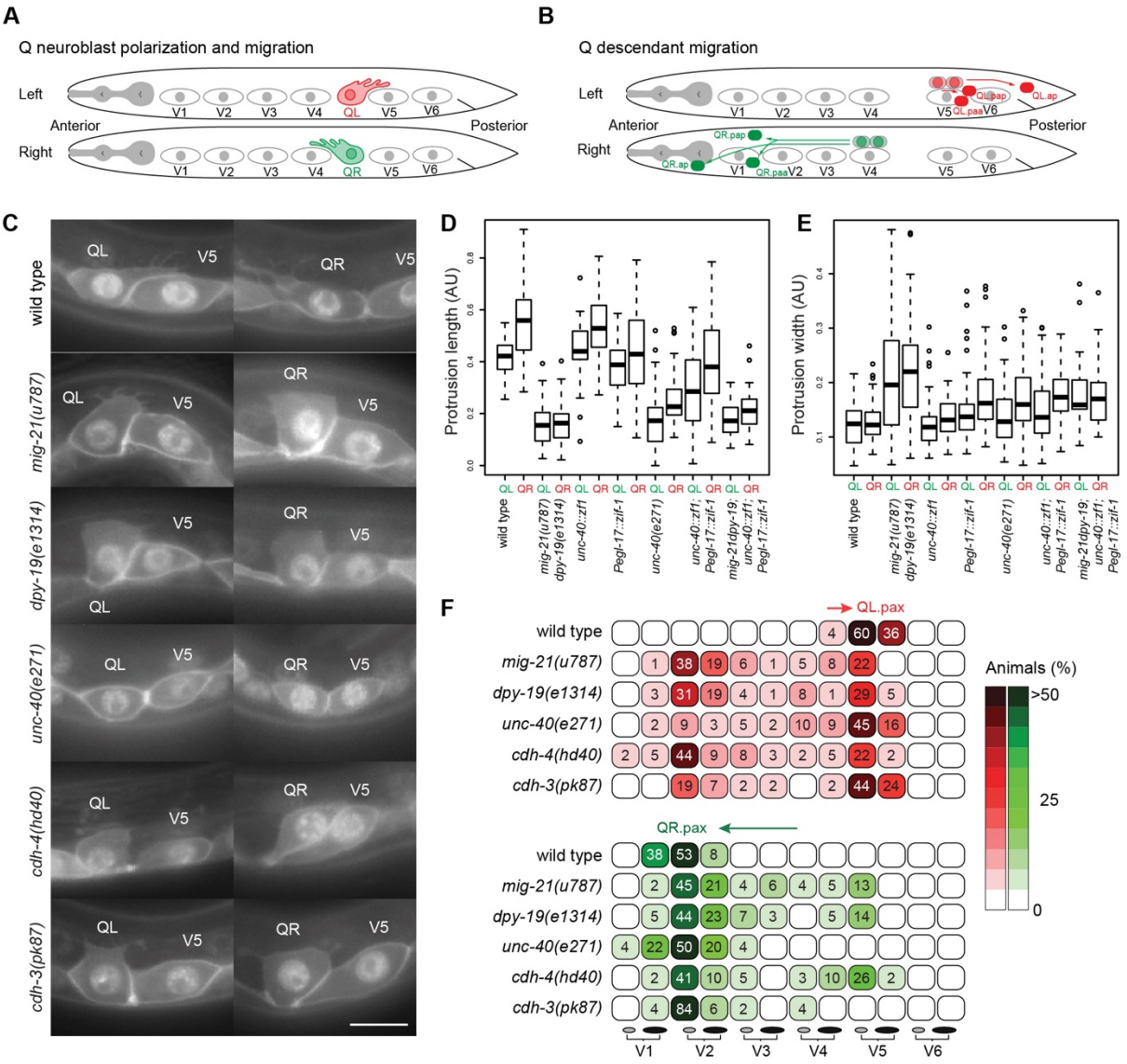

Figure S1. Polarization and migration of the Q neuroblasts and their descendants. (**A**) Schematic overview of the initial polarization and migration of the QL and QR neuroblasts. QL forms a lamellipodium-like protrusion towards the posterior and QR towards the anterior. After stable protrusion formation, the QL and QR cell bodies migrate to positions dorsal to V5 and V4 respectively. (**B**) After migration, QL and QR undergo an identical pattern of division, generating three neurons and two cells that undergo apoptosis. On the left side, the QL.p descendants remain close to the position of QL division, while the QL.a descendant QL.ap migrates to a position in the tail. On the right side, both the QR.a and QR.p descendants migrate anteriorly. (**C**) Representative images of Q neuroblast polarization in wild type and polarity mutants (1-2 hours after hatching). Anterior is left and dorsal is up. Scale bar is 10 μm. Quantification of protrusion length (**D**) and protrusion width (**E**) in wild type and polarity mutants (1-2 hours after hatching). (**F**) Final position of the Q. descendants Q.paa and Q.pap (Q.pax) relative to the seam cells. Arrows indicate direction of migration. Numbers and color coding represent percentages, n > 45. See Table S1 for statistical analysis of Q.pax position.

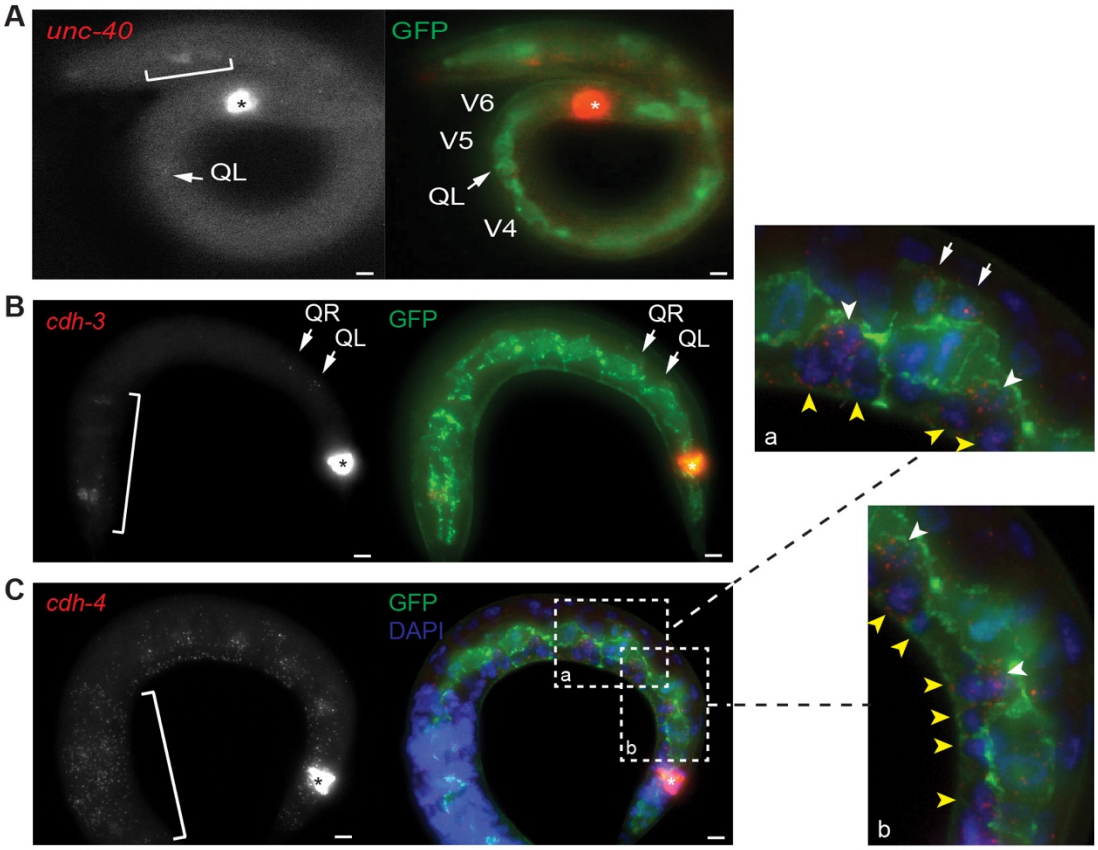

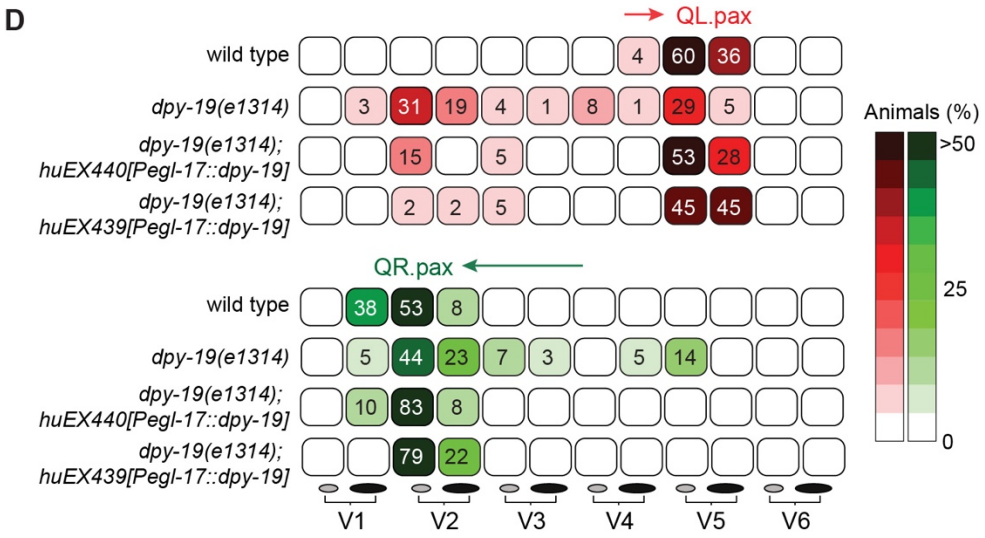

Figure S2. Expression patterns of *unc-40*, *cdh-3* and *cdh-4*. (A, B, C) smFISH at 1-2 hours after hatching. The Q neuroblasts and seam (V) cells are labeled with GFP (heIs63). Arrows indicate the Q neuroblasts, brackets expression in the head region and asterisk expression of the co-injection marker. (**C a**, **b**) Higher magnification images showing expression in the Q neuroblasts (white arrows), juvenile ventral cord neurons (yellow arrowheads) and P cells (white arrowheads). Anterior is left and dorsal is up. Scale bars are 5 μm. (**D**) Final position of the Q. descendants Q.paa and Q.pap (Q.pax) relative to the seam cells. Arrows indicate direction of migration. Numbers and color coding represent percentages, n > 40. See Table S1 for statistical analysis of Q.pax position.

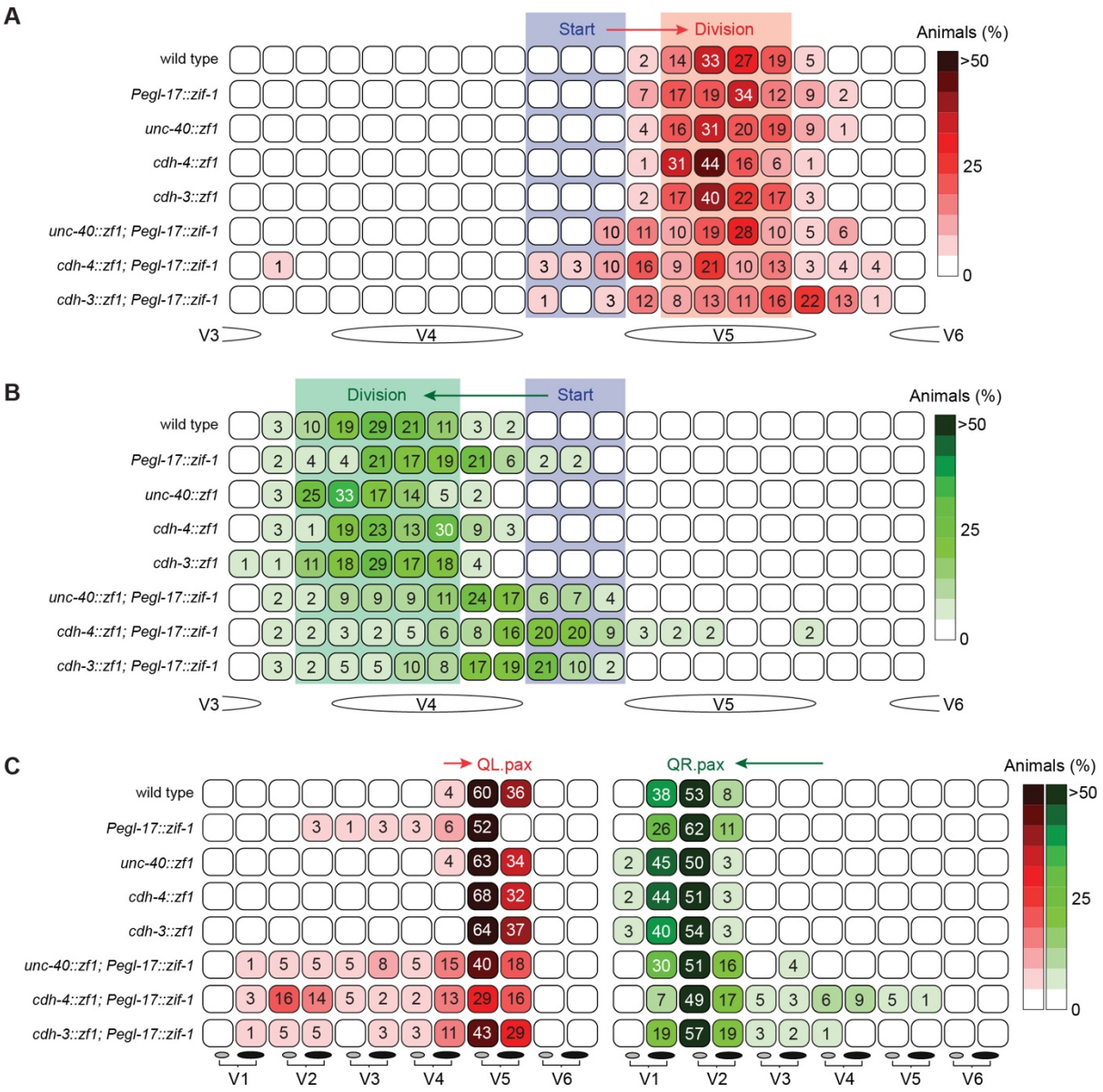

Figure S3. Q lineage specific depletion of UNC-40, CDH-4 and CDH-3. Quantification of QL (**A**) and QR (**B**) division position in animals in which *unc-40*, *cdh-4* and *cdh-3* are endogenously tagged with the *zf-1* sequence, and in which ZIF-1 is specifically expressed in the Q neuroblast lineage (*Pegl-17::zif-1*). Blue area represents the starting point of the migration and the red and green boxes the point where QL and QR divide in wild type animals. Numbers and color coding represent percentages, n > 45. (**C**) Final position of the Q. descendants Q.paa and Q.pap (Q.pax) relative to the seam cells. Arrows indicate direction of migration. Numbers and color coding represent percentages, n > 25. See Table S1 for statistical analysis of Q division position and Q.pax position.

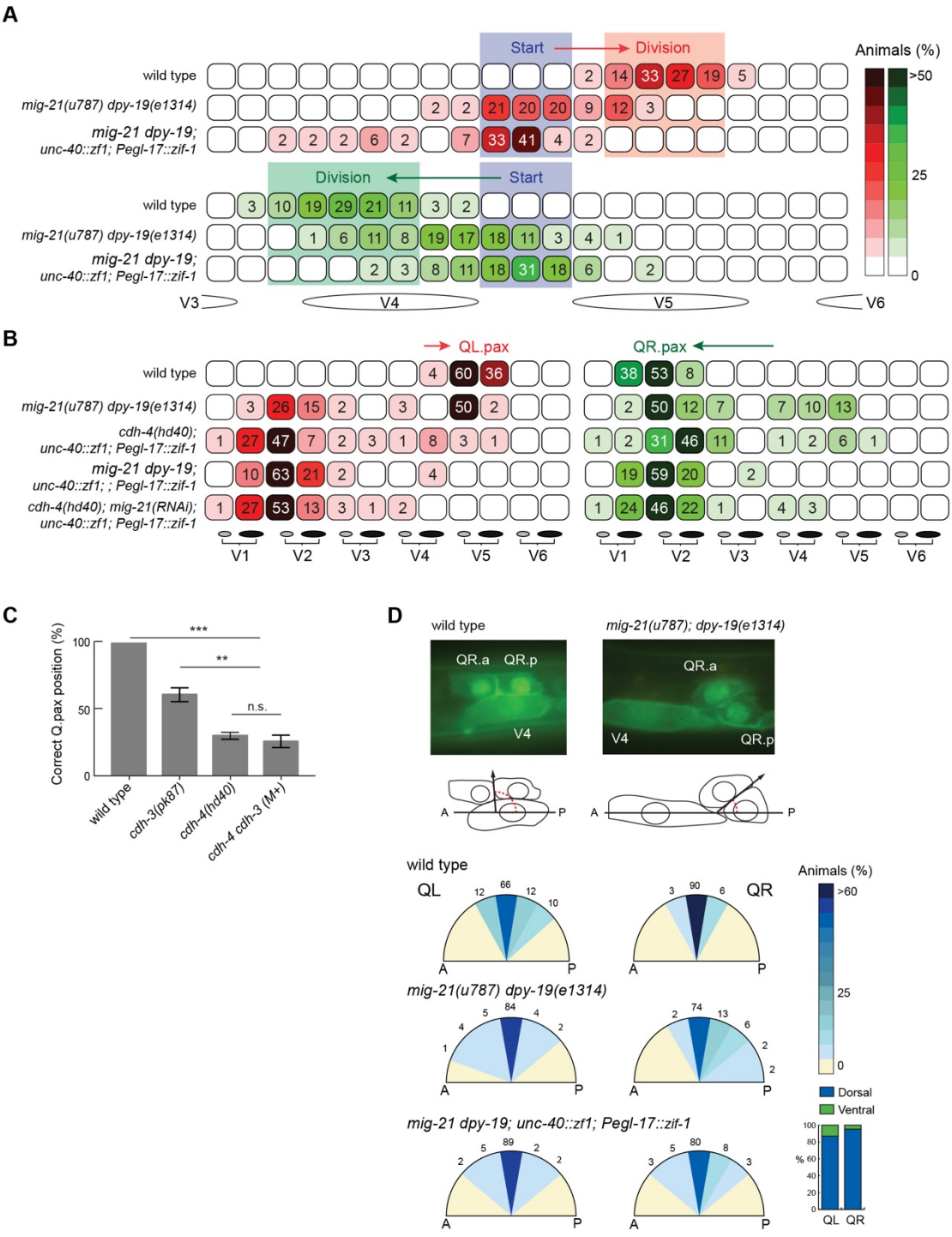

Figure S4. Polarization and migration of the Q neuroblasts and their descendants in the combined absence of polarity pathways. (**A**) Quantification of QL and QR division position in *mig-21(u787) dpy-19(e1314)* double mutants combined with Q lineage specific depletion of UNC-40 (*unc-40::zf-1; Pegl-17::zif-1*). Blue area represents the starting point of the migration and the red and green boxes the point where QL and QR divide in wild type animals. Numbers and color coding represent percentages, n > 50. (**B**) Final position of the Q. descendants Q.paa and Q.pap (Q.pax) relative to the seam cells. *mig-21* was knocked down by feeding RNAi. Arrows indicate direction of migration. Numbers and color coding represent percentages, n > 50. See Table S1 for statistical analysis of Q division position and Q.pax position. (**C**) Quantification of Q.pax position in *cdh-3(pk87)* and *cdh-4(hd40)* single and

maternally rescued (M+) double mutants. Numbers represent mean ± SD from three independent experiments (each n > 50). **p < 0.003, ***p < 0.0004, n.s., not significant (Student's t-test). (**D**) Quantification of the division plane of QL and QR. In wild type, a line through the point of contact between Q.a and Q.p is at a 90^{o} angle with the anteroposterior axis. In *mig-21(u787) dpy-19(e1314)* double mutants, the orientation of the Q division is more variable. Numbers and color coding represent percentages, n > 50. When UNC-40 is depleted (*unc-40::zf-1; Pegl-17::zif-1*) in *mig-21 dpy-19* double mutants, the Q neuroblasts occasionally divide ventral to the seam cells (bar diagram).

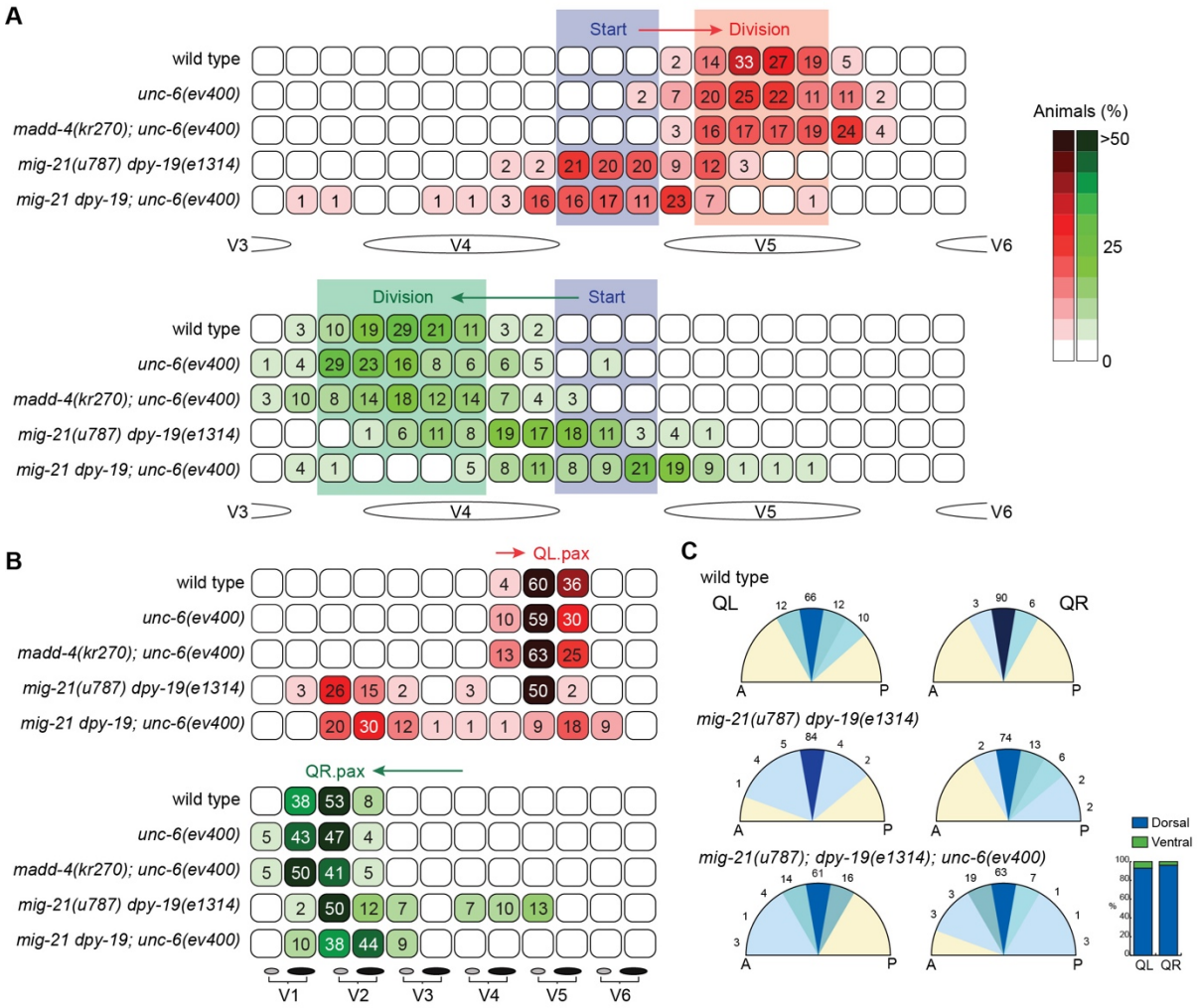

Figure S5. Polarization and migration of the Q neuroblasts and their descendants in the absence of the UNC-40 ligands UNC-6 and MADD-4. (**A**) Quantification of QL and QR division position. Blue area represents the starting point of the migration and the red and green boxes the point where QL and QR divide in wild type animals. Numbers and color coding represent percentages, n > 33. (**B**) Final position of the Q. descendants Q.paa and Q.pap (Q.pax) relative to the seam cells. Arrows indicate direction of migration. Numbers and color coding represent percentages, n > 47. See Table S1 for statistical analysis of Q division position and Q.pax position. (**C**) Quantification of the division plane of QL and QR. In wild type, a line through the point of contact between Q.a and Q.p is at a 90° angle with the anteroposterior axis. In *mig-21(u787) dpy-19(e1314)* double mutants and *mig-21 dpy-19*; *unc-6(ev400)* triple mutants, the orientation of the Q division is more variable. Numbers and color coding represent percentages, n > 50. In *mig-21 dpy-19*; *unc-6* triple mutants, the Q neuroblasts occasionally divide ventral to the seam cells (bar diagram).

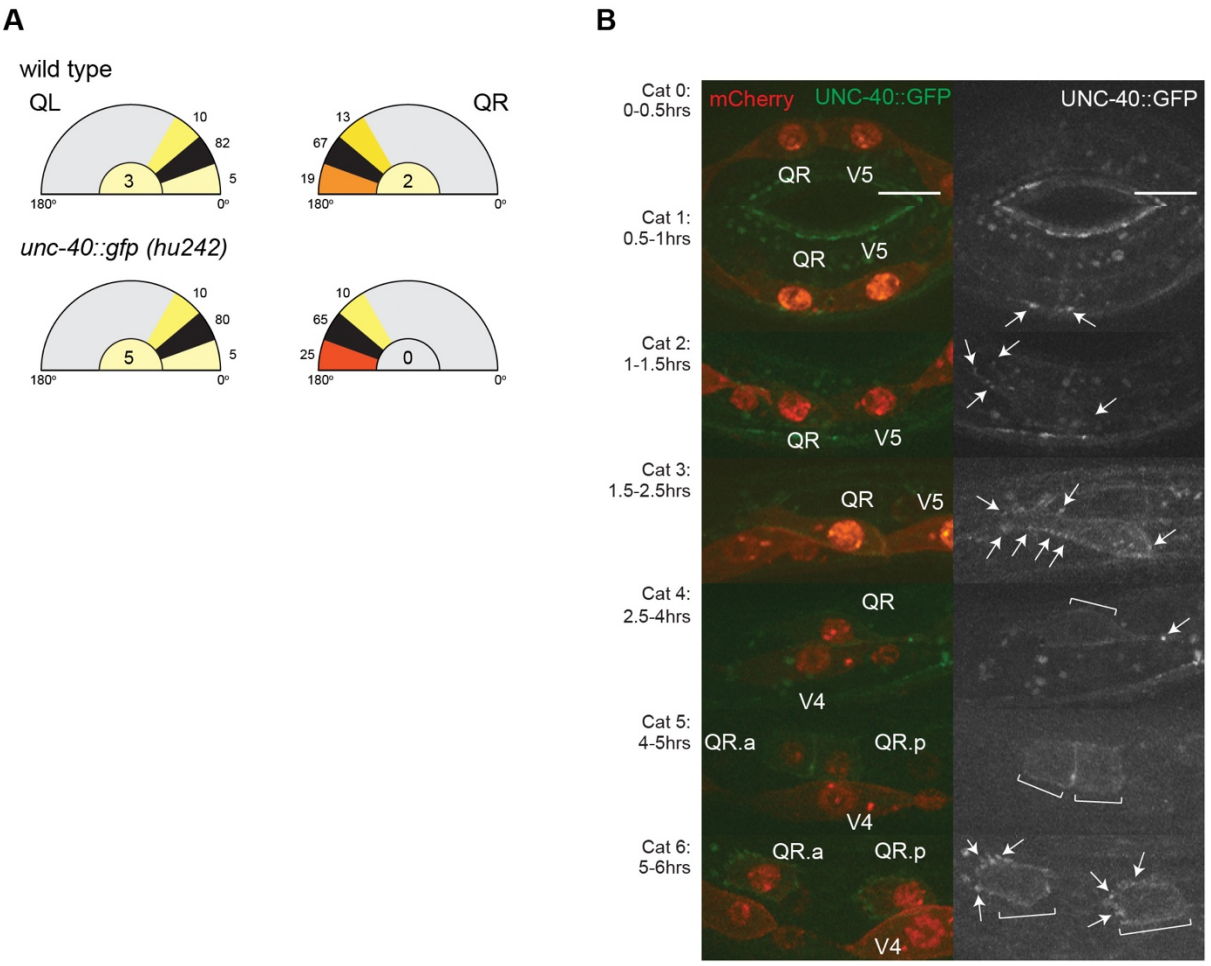

Figure S6. Endogenous UNC-40::GFP expression. (**A**) Quantification of protrusion formation and protrusion direction in wild type and *unc-40::gfp(hu242)* at 1-2 hours after hatching. Numbers and color coding represent percentages, n > 20. The percentage of cells that fail to form a major protrusion is indicated in the center of the polar graphs. See Table S1 for statistical analysis of protrusion formation and direction. (**B**) Representative images of UNC-40::GFP localization during polarization, migration and division (indicated by category and time after hatching). The plasma membrane and nucleus of the Q neuroblasts and seam (V) cells are labeled with mCherry (*huIs166*). UNC-40::GFP punctae are indicated by arrows. Brackets indicate diffuse UNC-40::GFP localization at the plasma membrane. Anterior is left and dorsal up. Scale bar is 10 μm.

Supplemental Tables

Table S1. Statistical analysis of Q polarization.
Click here to Download Table S1

Table S2. Statistical analysis of Q position of division
Click here to Download Table S2

Table S3. Statistical analysis of Q.pax position
Click here to Download Table S3

Table S4. Transgenic mosaic analysis to determine the site of action of *dpy-19*

Genotype	**Body shape**	**Percentage Q.pax migration defect***
dpy-19(e1314); huEx439[Pegl-17::dpy-19]		
Transgenic	Dpy	35.3 ± 5.0**
Transgenic	WT	21.3 ± 7.0
Non-transgenic siblings	Dpy	59.0 ± 5.6
dpy-19(e1314); huEx440[Pegl-17::dpy-19]		
Transgenic	Dpy	20.3 ± 4.0**
Transgenic	WT	7.90 ± 0.1
Non-transgenic siblings	Dpy	66.9 ± 8.2

Expression of wild type *dpy-19* in the Q neuroblast lineage of *dpy-19(e1314)* mutants rescues Q.pax migration (Fig. S2). However, in some of the transgenic animals, the Dpy phenotype is rescued as well. This indicates that despite the specificity of the *egl-17* promoter for the Q cell lineage, these transgenes may display a low level of *dpy-19* expression in the hypodermis. To circumvent this problem, we made use of the fact that extra-chromosomal transgenes are frequently lost during somatic cell divisions, leading to mosaic expression of the transgene. Using this approach, we found that transgenic mosaics that remain Dpy still show significant rescue of Q.pax migration, supporting our conclusion that *dpy-19* functions cell autonomously in the Q cell lineage. * mean ± SD. **t-test siblings versus Dpy: p=0.0056 and 0.0034 for *huEx439* and *huEx440*, respectively.

Table S5. Primers and oligonucleotides

	Sequence
***dpy-19* expression construct**	
dpy-19 FW	GGGGACAAGTTTGTACAAAAAAGCAGGCTATGGCAAAGAAACCCAAGAATTC
dpy-19 RV	GGGGACCACTTTGTACAAGAAAGCTGGGTTTCAGATTTTCAAAACAATATAATTCCT
Guide RNAs zf1 tagging	
unc-40	CCTCCTATTGCGAGATGTCTTGATGGATAAGTAATAATAATCGTTTAAGAGCTATGCTGG
cdh-4	CCTCCTATTGCGAGATGTCTTGGTGAATTAAAGAAATACTGAGTTTAAGAGCTATGCTGG
cdh-3	CCTCCTATTGCGAGATGTCTTGTAGAGACGGGCACATTAATAGTTTAAGAGCTATGCTGG
ssODN zf1 repair templates	
unc-40	ACAACAATTACAGCACAATTTGCATTTTGAGACGAGTATGGATAAGACAGAATACAAAACGCGACTTTGTGATGCGTTCCGCCGTGAAGGATACTGCCCGTACAACGACAATTGCACATATGCTCACGGACAAGATGAGCTGAGAGTTCCGAGATAATAATAATCTAGTATTTTTTTGATAATTTGAATTATTAATTTTG
cdh-4	TTTGATGATATAGACGAAGAAGTCAACATTCACATCTCTACAGAATACAAAACGCGACTTTGTGATGCGTTCCGCCGTGAAGGATACTGCCCGTACAACGACAATTGCACATATGCTCACGGACAAGATGAGCTGAGAGTTCCGAGATAATAACATTCAGTATTTCTTTAATTCACAATTTCTCAA
cdh-3	CTGCACCATCTTACCGTAGAGACGGGCACATTAATATAGCTTACTTAACAGAATACAAAACGCGACTTTGTGATGCGTTCCGCCGTGAAGGATACTGCCCGTACAACGACAATTGCACATATGCTCACGGACAAGATGAGCTGAGAGTTCCGAGATAGAGATATTTTATTTTCATCATTTTCGATTCATTTTTACGGGTT
SEC cassette cloning	
unc-40 sgRNA	GTAATACGACTCACTATAGGATGGATAAGTAATAATAATCGTTTTAGAGCTAGAAATAGC
dpy-19 sgRNA	GTAATACGACTCACTATAGGAAATAGTTTATAATGCTAATGTTTTAGAGCTAGAAATAGC
reverse sgRNA primer	AAAAGCACCGACTCGGTGC
HA 1 *dpy-19* FW	ACGTTGTAAAACGACGGCCAGTCGCCGGCAACAGTTGAATGTCAAGGGAGAA
HA 1 *dpy-19* RV	CATCGATGCTCCTGAGGCTCCCGATGCTCCGATTTTCAAAACAATATAATTTCTATTAGC
HA 2 *dpy-19* FW	CGTGATTACAAGGATGACGATGACAAGAGATGATTTTTTTCTATTTTGTTTTTAAATTTA
HA 1 *dpy-19* RV	GGAAACAGCTATGACCATGTTATCGATTTCTTTAGGCGGAAACCTCAGAC
HA 1 *unc-40* FW	ACGTTGTAAAACGACGGCCAGTCGCCGGCACGGTGGACGGCAAGTTCCAGTTGGAAGAGC
HA 1 *unc-40* RV	CATCGATGCTCCTGAGGCTCCCGATGCTCCCTTATCCATACTCGTCTCAAAATGCAAATT
HA 2 *unc-40* FW	CGTGATTACAAGGATGACGATGACAAGAGATAATAATAATCTGGTATTTTTTTGATAATT
HA 1 *unc-40* RV	GGAAACAGCTATGACCATGTTATCGATTTCGGATGTTAATCTGACAACTCTCATCTCC

Supplemental Movies

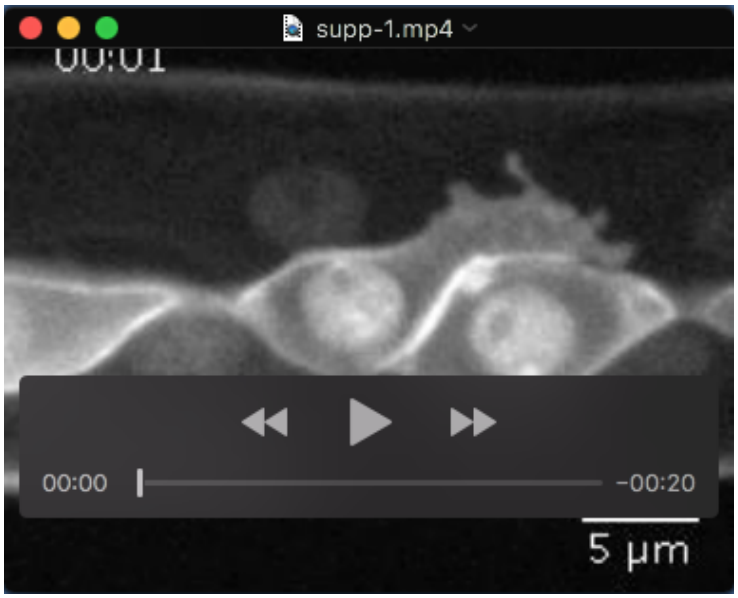

Movie 1. Live time-lapse confocal imaging of wild type animals expressing plasma membrane and nuclear localized GFP in QL and the seam cells (transgene *heIs63*). Anterior is left. Images were acquired every minute for a total duration of 1.5 hours. Movies are played at 5 frames per second.

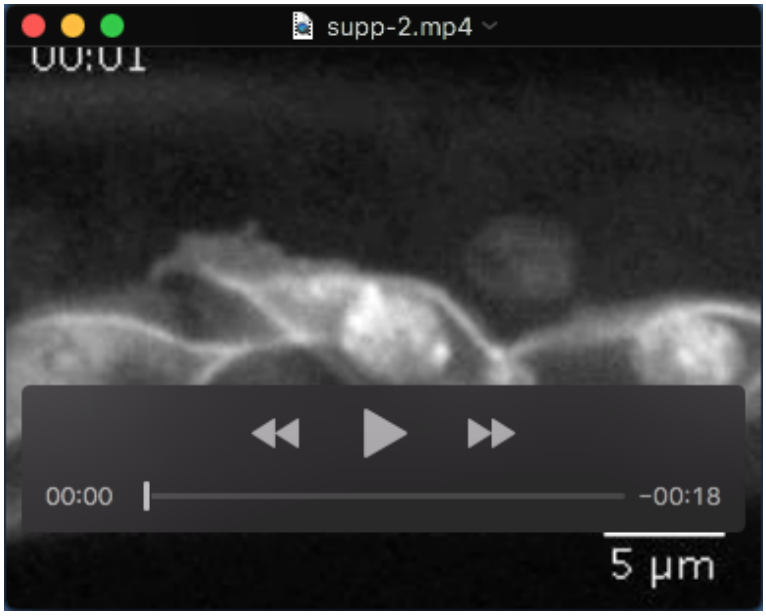

Movie 2. Live time-lapse confocal imaging of wild type animals expressing plasma membrane and nuclear localized GFP in QR and the seam cells (transgene *heIs63*). Anterior is left. Images were acquired every minute for a total duration of 1.5 hours. Movies are played at 5 frames per second.

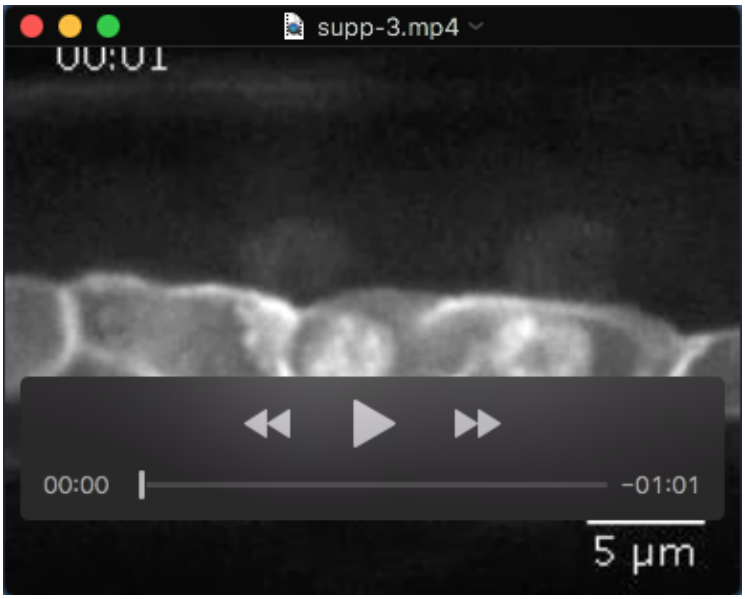

Movie 3. Live time-lapse confocal imaging of *cdh-4(hd40)* animals expressing plasma membrane and nuclear localized GFP in QL and the seam cells (transgene *heIs63*). A nterior is left. Images were acquired every minute for a total duration of 5 hours. Movies are played at 5 frames per second.

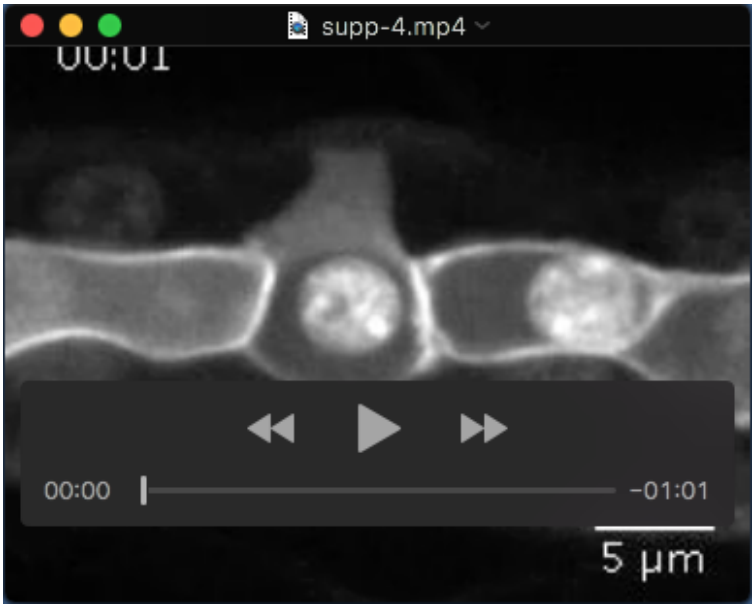

Movie 4. Live time-lapse confocal imaging of *cdh-4(hd40)* animals expressing plasma membrane and nuclear localized GFP in QR and the seam cells (transgene *heIs63*). Anterior is left. Images were acquired every minute for a total duration of 5 hours. Movies are played at 5 frames per second.

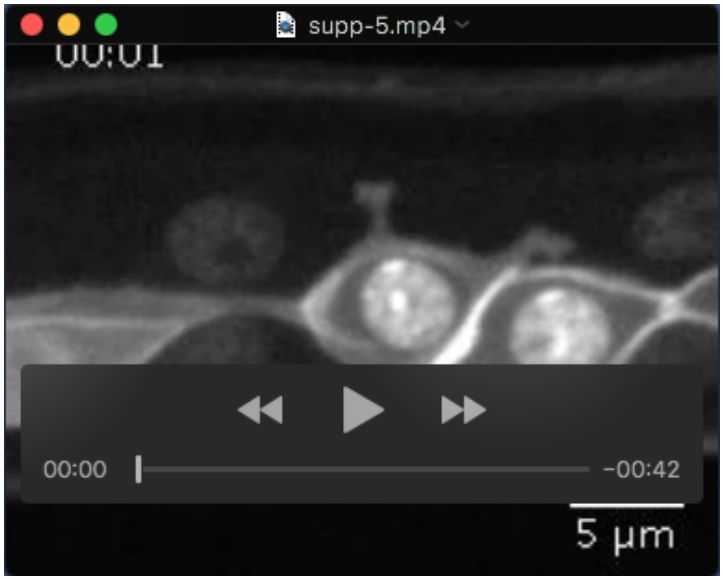

Movie 5. Live time-lapse confocal imaging of *cdh-3(pk87)* animals expressing plasma membrane and nuclear localized GFP in QL and the seam cells (transgene *heIs63*). Anterior is left. Images were acquired every minute for a total duration of 3.5 hours. Movies are played at 5 frame s per second.

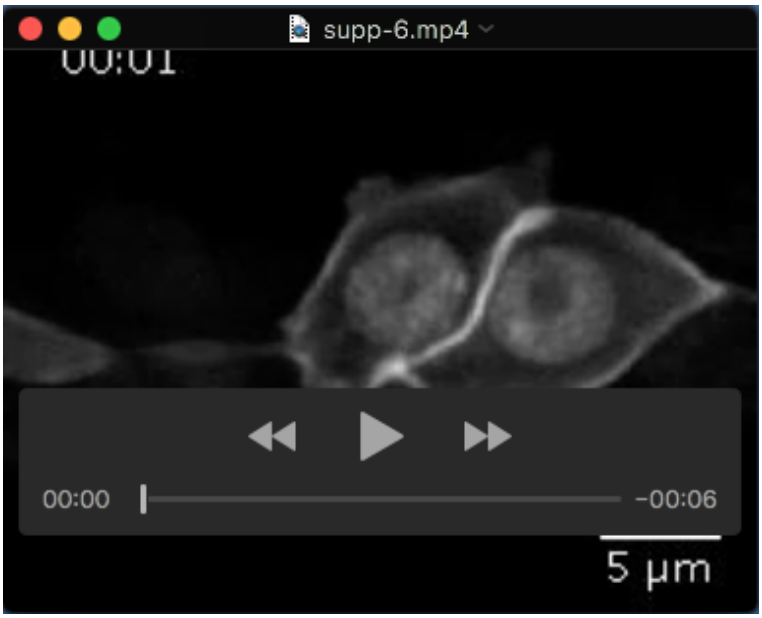

Movie 6. Live time-lapse confocal imaging of *unc-40(e271)* animals expressing plasma membrane and nuclear localized GFP in QL and the seam cells (transgene *heIs63*). Anterior is left. Ima ges were acquired every minute for a total duration of 1 hour. Movies are played at 5 frames per second.

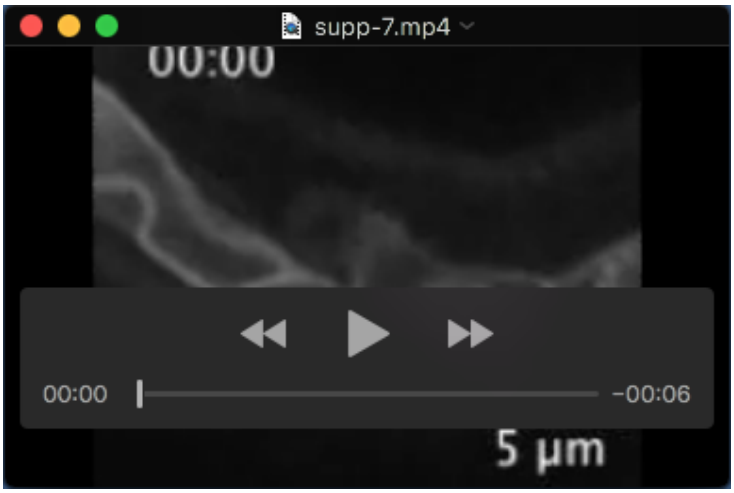

Movie 7. Live time-lapse confocal imaging of *unc-40(hu226[unc-40::zf1]); mig-21(u787) dpy-19(e1314); huIs181[Pegl-17::zif-1-SL2-mcherry; Pmyo-2::mcherry]* animals expressing plasma membrane and nuclear localized GFP in QL and the seam cells (transgene *heIs63*). Anterior is left. Images were acquired every 10 minutes for a total duration of 3 hours. Movies are played at 3 frames per second.

Movie 8. Live time-lapse confocal imaging of *unc-40(hu226[unc-40::zf1]); mig-21(u787) dpy-19(e1314); huIs181[Pegl-17::zif-1-SL2-mcherry; Pmyo-2::mcherry]* animals expressing plasma membrane and nuclear localized GFP in QR and the seam cells (transgene *heIs63*). Anterior is left. Images were acquired every 10 minutes for a total duration over 4.5 hours. Movies are played at 3 frames per second.